HHS Public Access

Author manuscript

Cell. Author manuscript; available in PMC 2022 February 18.

Published in final edited form as:

Cell. 2021 February 18; 184(4): 1017–1031.e14. doi:10.1016/j.cell.2021.01.016.

Human gut mycobiota tune immunity via CARD9-dependent induction of anti-fungal IgG antibodies

Itai Doron[1,2], **Irina Leonardi**[1,2], **Xin V. Li**[1,2], **William D. Fiers**[1,2], **Alexa Semon**[1,2], **Meghan Bialt-DeCelie**[1,2], **Mélanie Migaud**[3], **Iris H. Gao**[1,2,5], **Woan-Yu Lin**[1,2,5], **Takato Kusakabe**[1,2], **Anne Puel**[3], **Iliyan D. Iliev**[1,2,4,5,6,*]

[1]Gastroenterology and Hepatology Division, Joan and Sanford I. Weill Department of Medicine, Weill Cornell Medicine, New York, NY 10021, USA

[2]The Jill Roberts Institute for Research in Inflammatory Bowel Disease, Weill Cornell Medicine, New York, NY 10021, USA

[3]Laboratory of Human Genetics of Infectious Diseases Laboratory, INSERM UMR 1163, University of Paris, Imagine Institute, 75015 Paris, France

[4]Department of Microbiology and Immunology, Weill Cornell Medicine, New York, NY 10065, USA

[5]Immunology and Microbial Pathogenesis Program, Weill Cornell Graduate School of Medical Sciences, Weill Cornell Medicine, Cornell University, New York, NY 10065, USA

[6]Lead contact

SUMMARY

Antibodies mediate natural and vaccine-induced immunity against viral and bacterial pathogens, whereas fungi represent a widespread kingdom of pathogenic species for which neither vaccine nor neutralizing antibody therapies are clinically available. Here, using a multi-kingdom antibody profiling (multiKAP) approach, we explore the human antibody repertoires against gut commensal fungi (mycobiota). We identify species preferentially targeted by systemic antibodies in humans, with *Candida albicans* being the major inducer of antifungal immunoglobulin G (IgG). Fungal colonization of the gut induces germinal center (GC)-dependent B cell expansion in extraintestinal lymphoid tissues and generates systemic antibodies that confer protection against disseminated *C. albicans* or *C. auris* infection. Antifungal IgG production depends on the innate immunity regulator CARD9 and $CARD9^{+}CX3CR1^{+}$ macrophages. In individuals with invasive candidiasis, loss-of-function mutations in *CARD9* are associated with impaired antifungal IgG responses.

*Correspondence: iliev@med.cornell.edu.

AUTHOR CONTRIBUTIONS

I.D. and I.D.I. conceived and designed experiments. I.D., I.L., X.V.L., W.D.F., A.S., M.B.-D., T.K., I.H.G., and W.-Y.L. performed experiments. I.D., M.B.-D., and A.S. performed ITS sequencing and analysis. I.D. and I.D.I. generated figures and legends from analyzed data. A.P. and M.M. provided serum samples, performed genotyping, and contributed to experiment interpretation. I.D. and I.D.I. wrote the manuscript.

SUPPLEMENTAL INFORMATION

Supplemental information can be found online at https://doi.org/10.1016/j.cell.2021.01.016.

DECLARATION OF INTERESTS

Cornell University has filed a provisional patent application covering inventions described in this manuscript.

These results reveal an important role of gut commensal fungi in shaping the human antibody repertoire through CARD9-dependent induction of host-protective antifungal IgG.

Graphical Abstract

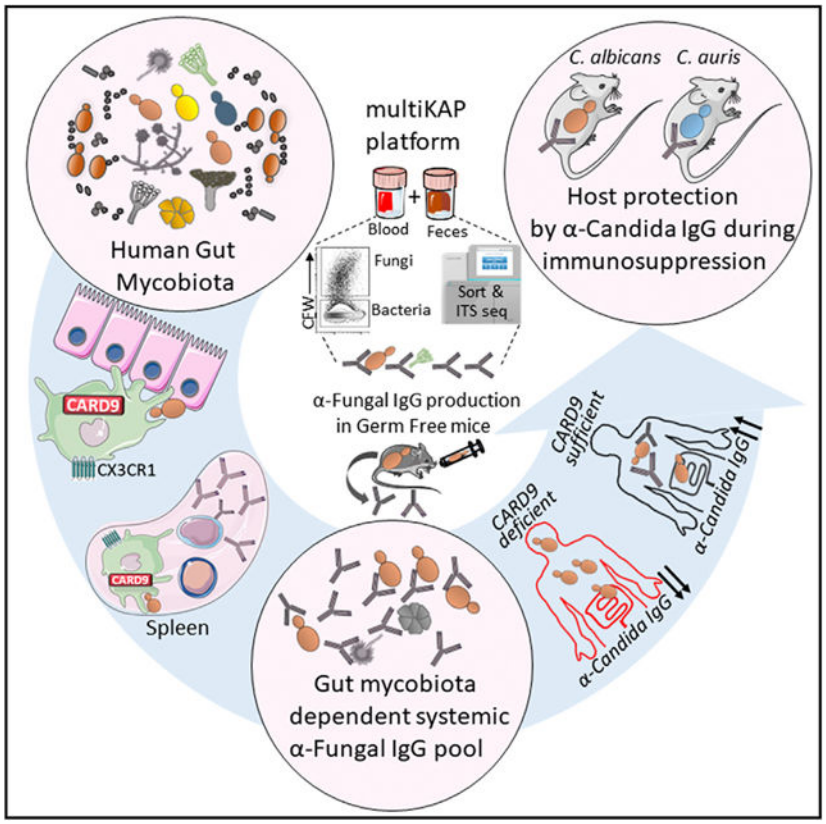

In Brief

Doron et al. present evidence that commensal fungi in the human gut shape antibody responses in the blood to protect the host from systemic lethal fungal infections. The innate immunity regulator CARD9 and CARD9+CX3CR1+ macrophages play an important role in antifungal IgG production, which is decreased in CARD9-deficient patients.

INTRODUCTION

The intestinal fungal community (mycobiota) is a highly immuno-reactive component of the microbiota with important implications for host immunity (Bacher et al., 2019; Leonardi et al., 2018; Li et al., 2018; Richard and Sokol, 2019; Shao et al., 2019; Tso et al., 2018). At the same time, the gut mycobiota are a reservoir of evolving fungal species from which serious infections can arise (Fan et al., 2015; Tso et al., 2018; Zhai et al., 2020). Advances in modern medicine, such as immunosuppressive therapy, chemotherapy, and organ transplantation, have contributed to a massive increase in deadly fungal infections affecting millions of people worldwide (Brown et al., 2012). These infections are often caused by systemic translocation of *Candida* species from the gut (Fan et al., 2015; Zhai et al., 2020).

The combination of a limited number of antifungal drugs and global emergence of multidrug-resistant *Candida* species renders these infections highly lethal, with mortality rates as high as 50% (Brown et al., 2012). Despite years of efforts to produce a much-needed antifungal vaccine through fungal antigen immunization (Casadevall and Pirofski, 2003, 2012; Edwards et al., 2018; Martinez et al., 2004; Montagnoli et al., 2003; Pachl et al., 2006; Wüthrich et al., 2012), fungi still represent a wide-spread kingdom of deadly pathogens for which neither vaccines nor neutralizing antibody therapies are clinically available (Fisher et al., 2012; Garcia-Solache and Casadevall, 2010; Rudkin et al., 2018).

Most antibacterial and antiviral vaccines available today are rooted in boosting antibody-mediated immunity (Plotkin, 2010). Notably, systemic immunoglobulin G (IgG) antibodies with broad specificity for intestinal bacteria are an important component of host protection against systemic bacterial infections of intestinal origin (Ansaldo et al., 2019; Koch et al., 2016). In contrast, IgG antibody responses to several intestinal fungi or their cell wall components are known to occur during gastrointestinal disease (Leonardi et al., 2018, 2020; Riente et al., 2004; Standaert-Vitse et al., 2006; Yang et al., 2017) and are generally perceived as disease markers rather than protective responses. However, antibodies against fungal β-glucan and other fungal antigens have been detected recently in serum of healthy humans (Chiani et al., 2009; Huertas et al., 2017), raising several important questions regarding the function of antifungal antibodies, the species that induce them, and the mechanisms governing their induction and regulation. We hypothesized that fungal species of the gut mycobiota play a critical role in shaping the host antibody repertoire by promoting induction of host-protective antifungal antibodies.

RESULTS

To explore the antibody pool against gut mycobiota, we established a multistep flow cytometry-based technique for multi-kingdom antibody profiling (multiKAP) (Figure 1A) that uses the native reservoir of gut commensal fungi and bacteria in fecal material as potential epitopes for antibody binding. Serum from the same host is applied to the fecal sample to allow systemic antibody binding to intestinal microbes that are also already bound to the luminally secreted antibodies present in the feces (Figure 1A). Live microbes labeled with a DNA-binding dye (SYBR Green; $SYBR^{hi}$) in mouse feces are distinguished from dead microbes ($SYBR^{lo}$) in sterilized food and bedding by calibrating the assay against germ-free (GF) mouse feces (Figure 1B). In contrast to previously established microbial flow cytometry-based techniques (Ansaldo et al., 2019; Christmann et al., 2015; Fadlallah et al., 2019; Koch et al., 2016; Palm et al., 2014), multiKAP distinguishes fungi from the more abundant bacteria by their large cell size and the distinct presence of chitin in their cell walls (Figures 1B–1D). Size separation by centrifugation at 900 × *g*, followed by sorting of antibody-bound fungal and bacterial cells and isolation of their DNA for down-stream deep sequencing/analysis allows assignment of fungal identities, in addition to bacterial identities, in the same multiKAP assay (Figures 1D and 1E).

Co-staining of fecal microbes with Sybr and calcofluor-white (CFW; a chitin-binding dye) followed by flow cytometry analysis determined that 1%–2% of the microbes in mouse feces were fungal cells ($SYBR^{hi}CFW^{+}$; Figures 1C and S1A). To determine whether the gut

mycobiota are coated by antibodies of local secretory and/or systemic origin, we next analyzed the IgA- and IgG-bound fungal ($SYBR^{hi}CFW^{+}$) and bacterial ($SYB\text{-}R^{hi}CFW^{-}$) populations before and after fecal incubation with serum from the same mouse. Consistent with previously reported luminal IgA reactivity to intestinal bacteria in mice (Bunker et al., 2015; Koch et al., 2016; Palm et al., 2014), roughly half of the intestinal fungi identified by multiKAP were also bound by IgA independent of serum supplementation (Figures 1F and 1G), suggesting that systemic antibodies make a small contribution to the antifungal IgA repertoire in mice. Notably, a population of intestinal fungi were bound by IgG found exclusively in the blood (Figures 1F, 1G, and S1A; +wild-type [WT] serum) because no IgG-bound fraction of the mycobiota was present in the intestinal lumen under steady-state conditions (Figures 1F, 1G, and S1A; −serum). A similar binding pattern was observed when feces from Ig-deficient $Rag2^{-/-}$ mice were used as a gut fungal source to avoid prior IgA epitope coating (Figure S1B). Antifungal IgG binding was absent upon incubation with serum from B cell-deficient $\mu MT^{-/-}$ mice, which lack systemic antibodies, confirming the specificity of this assay (Figures 1F, 1G, and S1A; $+\mu MT^{-/-}$ serum). We also detected systemic antifungal IgM antibodies restricted to the blood (Figures 1F and 1G), supporting previous reports of involvement of the natural antifungal IgM repertoire in early immune responses during *Pneumocystis* or *Cryptococcus* infection (McClelland et al., 2010; Rapaka et al., 2010). Although antifungal IgM binding was similar upon incubation of specific pathogen-free (SPF) feces with GF and SPF serum, antifungal IgG binding was absent in GF serum-incubated SPF feces (Figures 1H–1K), indicating that induction of antifungal IgG, but not antifungal IgM, is gut microbiota dependent. Mice from different facilities that harbor compositionally different mycobiota (Doron et al., 2019) exhibit a variety of IgG binding, with our facility's "Ascomycota-high" mouse colony (Doron et al., 2019) and Taconic mice showing significantly higher antifungal IgG than mice from the Jackson Laboratories facility (Figure 1L). This phenomenon was independent of any detectable fungal pathology in the examined colonies or systemic fungal spread (Figures S1F and S1G). Given these findings and the negligible contribution of serum IgA to the antifungal IgA repertoire (Figures 1F and 1G), we focused on analyzing the gut microbiota-dependent systemic antifungal IgG response. Previous studies have observed that the IgG2b and IgG3 subtypes dominate the IgG response to commensal gut bacteria, with the IgG2b isotype binding the largest fraction of the bacteria (Koch et al., 2016). Although we observed a similar abundance of these two IgG isotypes (Figures S1C and S1D; Koch et al., 2016), IgG3 bound the largest fraction of the intestinal fungi (Figures 1M and 1N).

Fungi and bacteria cohabitate in the human intestine, where we found that fungal constituents of the microbiota are more prevalent (~2%) than initially predicted by metagenomics studies (Arumugam et al., 2011; Li et al., 2019; Figures 2A, 2B, and S1E). An initial multiKAP-based assessment of healthy human subjects determined that, despite substantial inter-individual variation, a large fraction of human intestinal fungi is bound by luminal IgA independent of serum addition (Figure 2C). Similar to mice, mycobiota-reactive IgG antibodies in healthy individuals were restricted to the serum (Figure 2C). MultiKAP assessment of these human subjects revealed that, along with a large proportion of all gut fungi bound to IgG and IgA ($IgG^{+}IgA^{+}$, ~50%) or neither antibody isotype ($IgG^{-}IgA^{-}$, ~25%), a significant population of fungi was only bound by IgG ($IgG^{+}IgA^{-}$, ~20%) (Figure

2D). These data demonstrate that a significant fraction of the gut mycobiota is recognized by systemic antifungal IgG antibodies in humans and mice. Furthermore, systemic mycobiota-reactive IgG antibodies are typically present in the serum of mice and healthy individuals, whereas antifungal IgA antibodies are mostly present in the gut.

To determine specific gut fungi that are preferentially coated or neglected by systemic human IgG antibodies, we coupled the multiKAP technique to ITS sequencing of gut fungal populations that were sorted from fecal material based on antibody binding (Figures 2D, S2A, and S2B). ITS sequencing revealed a variety of commensal, environmental, and food-associated fungi (Figure 2E), consistent with previous studies (Nash et al., 2017; Sokol et al., 2017). As noted above, we distinguished three populations of intestinal fungi (IgG^+IgA^+, IgG^+IgA^-, and IgG^-IgA^-) by multi-KAP, where all luminal IgA-bound fungi were also recognized by systemic IgG. Among these, the IgG-bound mycobiota (IgG^+IgA^+ and IgG^+IgA^-) were enriched for *C. albicans* (as determined by the positive coating index [CI]) (Kau et al., 2015; Figure S2C), whereas gut fungi not bound by either antibody pool (IgG^-IgA^-) were represented by skin- and food-associated fungal species such as *M. restricta* and *S. cerevisiae*, which rarely cause gut-disseminated infections in humans (Brown et al., 2012; Fan et al., 2015; Zhai et al., 2020; Figures 2F–2H and S2D). Other fungi detected by this approach were distributed equally in antibody-bound and unbound fractions and, thus, were not considered to be preferentially coated by anti-fungal antibodies (Figures 2F, 2G, and S2D). These data indicate that the systemic antifungal IgG antibody repertoire in healthy individuals is primarily characterized by preferential specificity to commensal *Candida*.

Candida is one of the most common genera of fungal commensals in the healthy human gastrointestinal tract (Li et al., 2019; Nash et al., 2017; Sokol et al., 2017) but also harbors the main opportunistic pathogens that cause disseminated fungal infections with high attributable morbidity and mortality in humans (Brown et al., 2012; Fan et al., 2015; Zhai et al., 2020). Among other fungi, *C. albicans* has been implicated as a potent inducer of Th17 responses in humans and mice; it is bound by host antibodies and, thus, has the potential to induce protective immune responses or trigger inflammation in a context-dependent manner (Bacher et al., 2019; Conti et al., 2009; Huertas et al., 2017; Leonardi et al., 2018; Li et al., 2018; Moreno-Sabater et al., 2020; Shao et al., 2019; Standaert-Vitse et al., 2009). Although most studies of intestinal *C. albicans* have focused exclusively on innate and Th17-mediated immunity, humoral immunity to this commensal in the gut remains poorly understood. Given our finding that systemic antibodies preferentially coat gut *C. albicans*, we sought to characterize how systemic antibody responses to this intestinal fungus are mediated.

IgG antibody responses to intestinal microbes can originate by antigen-specific responses to a distinct organism or can be derived from pre-existing cross-reactive specificities (Ansaldo et al., 2019; Koch et al., 2016; Slack et al., 2009). To investigate these possibilities and identify gut fungi that induce systemic antifungal IgG responses, we performed fungal monocolonization of GF mice that lacked antibody responses to fungi before colonization (Figures 2I, 1H, and 1I). Among fungal species identified by multiKAP, *C. albicans* induced the most potent systemic IgG antibody response (Figure 2I). Notably, antibodies generated by intestinal colonization with *C. albicans* were not cross-reactive with environmental, food-derived, or skin-resident fungi such as *Saccharomyces*, *Aspergillus*, and *Malassezia* spp.

(Figure 2J), suggesting a potential specificity restricted to resident fungal antigens. These data further indicate that intestinal fungal colonization can induce systemic antifungal IgG antibodies that are not derived from pre-existing cross-reactive specificities and implicate *C. albicans* as the predominant intestinal fungal species triggering this response.

A better understanding of fungus-specific antibody induction is obscured by coexistence of fungi with a dynamic bacterial community whose composition profoundly influences colonization of, and immune responses induced by, newly introduced bacterial or fungal commensals (Fan et al., 2015; Hand et al., 2012; Kim et al., 2019; Leonardi et al., 2020; Zhai et al., 2020). Furthermore, mycobiota are variable, essential components of the gut microbial communities of SPF mice (Doron et al., 2019; Leonardi et al., 2018; Li et al., 2018), and systemic antifungal IgG antibodies are present in their serum during homeostasis (Figures 1F–1L). To avoid the influence of these confounding factors in our investigation into the mechanisms of antifungal antibody induction, we utilized altered Schaedler flora (ASF)-colonized mice that carry a defined set of bacteria but are mycobiota-free (Li et al., 2018; Schaedler et al., 1965). In this setting, intestinal colonization with *C. albicans* (preferentially coated by systemic IgG antibodies) induced strong production of systemic antifungal IgG antibodies without priming unspecific antibacterial IgG response, whereas *S. cerevisiae* (preferentially not coated by systemic IgG antibodies) induced a limited IgG response (Figures 3A and S3A). These findings further support the notion that specific gut fungi might play a dominant role in induction of systemic antifungal IgG antibodies.

IgG responses to intestinal bacteria have been attributed to gut-associated lymphoid tissue (GALT) (Ansaldo et al., 2019; Koch et al., 2016; Teng et al., 2016) and extra-intestinal systemic locations (Barbet et al., 2018; Zeng et al., 2016). To determine sites of B cell expansion and IgG class switch recombination (CSR) upon intestinal fungal colonization, gut-distal tissue (spleen) and GALT (mesenteric lymph nodes [mLNs] and Peyer's patches [PPs]) were obtained from fungus-colonized (*C. albicans*-colonized [+*Ca*] and *S. cerevisiae*-colonized [+*Sc*]) and fungus-free ASF (ASF) mice. Notably, *C. albicans* gut colonization induced a robust IgG CSR in the spleen but not in PPs or mLNs (Figure 3C). On the other hand, *S. cerevisiae* induced a limited CSR response at these sites (Figure 3C), consistent with its low capacity to induce systemic IgG antibodies (Figure 3A). These results were not attributable to any noticeable systemic fungal spread or acute reaction (Macpherson et al., 2000) to *C. albicans* colonization because no live fungi were detectable in multiple organs, whereas anti-*C. albicans* IgG antibodies appeared at 2 weeks and persisted after the initial colonization event (Figures S3D and S3E). Generation of high-specificity IgG is often driven by expansion of germinal center B (GC-B) cells (Barbet et al., 2018; Teng et al., 2016), which undergo many cycles of somatic hypermutation (SHM) that are associated with high-affinity and high titers of antibodies (Victora and Nussenzweig, 2012). Consistent with its ability to drive CSR, gut *C. albicans* induced potent splenic GC-B cell expansion and differentiation accompanied by transfer of *C. albicans* antigens (as assessed by sensitive DNA-based assay) to the spleen (Figures 3B and 3D). No significant differences were detected in the frequency of total splenic B cells between experimental groups (Figures S4B and S4C). Notably, adoptive transfer of antibody-producing splenic B cells from +*Ca* mice, but not antibody-deficient B cells or B cells from GF mice, protected highly susceptible $\mu MT^{+/-}$ mice against systemic candidiasis, suggesting a protective role of B cell-mediated

immunity against fungal infection (Figures 4A, 4B, S4A, and S4B). These data suggest that the gut commensal *C. albicans* induces systemic IgG production through expansion of GC-B cells in the spleen.

To determine the functional role of systemic antifungal IgG, we purified IgG antibodies from serum of GF mice, which normally lack systemic anti-commensal IgG antibodies in the absence of fungal or bacterial antigen exposure (Figures 1H and 1I), intestinally monocolonized with *C. albicans* (*C.alb*-IgG) or *S. cerevisiae* (*S.cer*-IgG) (Figure 4C). Antifungal antibodies obtained from *C. albicans* ex-GF mice have strong reactivity with *C. albicans*, whereas IgG antibodies from serum of *S. cerevisiae*-monocolonized mice demonstrate weaker reactivity with *S. cerevisiae* (Figures 4C and 2J).

We next explored the role of these antibodies during immunosuppression, where, among different fungi, *Candida* species are the main cause of morbidity and mortality in people, with the gut often being the fungus source (Brown et al., 2012; Zhai et al., 2020). Thus, *C.alb*-IgG or *S.cer*-IgG antibodies were transferred into SPF mice intestinally colonized with *C. albicans* and treated with the chemotherapy drug cyclophosphamide (Cyc) to induce immunosuppression and facilitate gut-to-system fungal dissemination and death (Figure S4B; Koh et al., 2008). In addition to severe leukopenia (Koh et al., 2008), Cyc treatment led to a dramatic decrease in antifungal IgG antibodies in the serum of mice (Figure S4C). Notably, *C.alb*-IgG transfer into these mice led to nearly complete survival 4 weeks after systemic fungal dissemination and significantly decreased kidney fungal burdens (Figures 4D and 4E), whereas *S.cer*-IgG transfer did not reduce infection mortality (Figures 4F and 4G). *Candida auris* is an emerging multidrug-resistant fungal pathogen that is a serious global health threat and is the cause of multiple nosocomial outbreaks worldwide that are associated with unusually high mortality rates (Eyre et al., 2018). Thus, we used our GF colonization protocol to generate antibodies against this multidrug-resistant fungal pathogen and test their efficacy. Notably, such generated antibodies (*C.aur*-IgG) protected mice against intravenous *C. auris* infection and death. *C.alb*-IgG antibody transfer was also protective but to a lower extent (diminishing only brain-disseminated candidiasis), suggesting some level of antibody selectivity even among fungi belonging to the same species (Figures 4H–4J). These results demonstrate that systemic antibodies to mycobiota generated through the gastrointestinal route protect the host against deadly systemic fungal infections of intestinal or non-intestinal origin. Moreover, this protection demonstrates the powerful effect of antifungal antibody immunity in the face of broad cellular immunity depression by chemotherapeutics.

Among genetic factors associated with fungal infections, CARD9 deficiency is the only known human genetic disorder that specifically leads to recurrent severe mucosal and systemic fungal infections without conferring bacterial, parasitic, or viral susceptibility (Cao et al., 2015; Glocker et al., 2009; Lionakis et al., 2014). CARD9 is required to activate nuclear factor κB (NF-κB)-based signaling downstream of the receptors Dectin-1, Dectin-2, and Mincle in innate immune cells, which, in turn, induces cytokine production and triggers cellular immunity against fungi (Cao et al., 2015; Drummond et al., 2015; LeibundGut-Landmann et al., 2007; Pérez de Diego et al., 2015; Roth and Ruland, 2013). A common polymorphism in *CARD9* is among the strongest genetic risk factors associated with

Crohn's disease, where increased anti-*S. cerevisiae* IgG antibodies (ASCA IgG) are a clinical marker of disease severity (Evans et al., 2011; Jostins et al., 2012; Rivas et al., 2011). Furthermore, *CARD9* deficiency has been associated with gut fungal dysbiosis (Lamas et al., 2016), revealing CARD9 signaling as a critical link between gut mucosal immunity and intestinal fungi. Interestingly, *Card9*-deficient ($Card9^{-/-}$) mice that were highly susceptible to systemic candidiasis originating from the gut upon Cyc treatment were unable to induce systemic antifungal IgG antibodies despite a high systemic *Candida* burden (Figures 5A–5C) and normal development of T and B cell subsets (Hsu et al., 2007; Figures S4H and S4I). In contrast, *Card9*-sufficient ($Card9^{+/+}$) mice that were more resistant to fungal infection with intestinal origin were able to generate systemic IgG antibodies against *C. albicans* (Figures 5A–5C). MultiKAP analysis of antifungal IgG antibodies demonstrated that the presence of a systemic antifungal IgG repertoire was strikingly dependent on the presence of CARD9 signaling (Figures 5D and 5E). These results suggest an unexpected role of CARD9 in induction of systemic anti-fungal IgG responses to intestinal fungi.

To investigate the mechanisms behind the observed CARD9-mediated antifungal IgG response, we intraperitoneally delivered heat-killed *C. albicans* to circumvent the extreme susceptibility of $Card9^{-/-}$ mice to systemic candidiasis (Drummond et al., 2015; Lionakis et al., 2014; Figures 5F–5K, S4D, and S4E). We found that IgG^+ B cell frequency among circulating B cells in the blood only increased significantly in response to *C. albicans* in $Card9^{+/+}$ mice (Figures 5F and 5G). In contrast to $Card9^{+/+}$ mice, $Card9^{-/-}$ mice were unable to induce an efficient anti-*C. albicans* IgG antibody response, and this corresponded with defective IgG^+ CSR and GC-B cell expansion in the spleen (Figures 5H–5K) but was not due to B cell-intrinsic or developmental defects in the absence of CARD9 (Figures S4F and S4G). These data indicate that the GC-dependent systemic antifungal IgG antibody response is dependent on CARD9.

Single-cell RNA sequencing (RNA-seq) analysis of a previously published dataset (Smillie et al., 2019) determined that *CARD9* expression in humans is restricted to several populations of phagocytes, such as macrophages, monocytes, and dendritic cells (DCs; Figure 6A). In mice, these populations include $CD103^+$ conventional DCs ($CD11b^-$ cDC1s and $CD11b^+$ cDC2s) and $CX3CR1^+$ mononuclear phagocytes (MNPs), cells described previously as providing an interface between the gut microbiota and anti-commensal immunoglobulin induction (Flores-Langarica et al., 2018; Kim et al., 2018; Koscsó et al., 2020; Takaki et al., 2018). Because $CX3CR1^+$ MNPs and the cDC2 subset represent the vast majority of C-type lectin receptor (CLR)/CARD9-expressing antigen-presenting cells, and a loss-of-function mutation in *CX3CR1* is associated with reduced antifungal IgG antibodies in humans (Li et al., 2018), we next set out to identify the potential involvement of $CX3CR1^+$ MNPs and cDC2 in induction of IgG with specificity for intestinal fungi. We crossed transgenic *Cd11c-Cre* mice with inducible floxed CX3CR1 ($Cx3cr1^{DTR}$) or cDC2 master regulator IRF4 ($IRF4^{fl/fl}$) mice to generate models of inducible $CX3CR1^+$ MNPs (ΔCX3CR1) and cDC2 (ΔIRF4) depletion, respectively (Figures S5A–S5D). MultiKAP analysis of serum IgG binding revealed that, relative to their respective Cre^- littermates, $CX3CR1^+$ MNPs, but not cDC2 depletion, abrogated the systemic anti-fungal IgG (Figures 6B and 6D). Intestinal colonization with *C. albicans* led to a reduction in IgG^+ frequency in the splenic B cell compartment of ΔCX3CR1 but not ΔIRF4 mice or littermate controls

(Figures 6C and 6E). To assess whether Syk-Card9-mediated antifungal signaling on CX3CR1^{+} MNPs is necessary for induction of antifungal humoral responses, we crossed transgenic *Cx3cr1-cre/ERT2*$^{+/-}$ mice with a strain carrying an inducible floxed spleen tyrosine kinase (Syk; *Syk*$^{fl/fl}$) to conditionally block Syk-dependent, Card9-mediated antifungal signaling in CX3CR1^{+} MNPs (CX3CR1$^{\Delta Syk}$ mice). We found that CX3CR1^{+} MNP-specific targeting of this pathway significantly reduced systemic antifungal IgG in CX3CR1$^{\Delta Syk}$ mice (Figure 6F). Furthermore, the increased frequency of splenic IgG^{+} B cells observed in *C. albicans*-colonized littermates was not observed in CX3CR1$^{\Delta Syk}$ mice (Figure 6G). Notably, a comparison of antifungal IgG binding in αβT cell-deficient *TCRβ*$^{-/-}$ demonstrated significant loss of antifungal IgG binding relative to αβT cell-sufficient counterparts (*TCRβ*$^{+/+}$), suggesting that CX3CR1^{+} MNPs mediate antifungal IgG induction through T cell-dependent mechanisms (Figure 6H). These data pinpoint CX3CR1^{+} MNPs as mediators of commensal fungus-induced systemic antifungal IgG.

Having established the necessity of Syk-Card9 signaling for induction of antifungal antibodies in mice, we next explored whether a similar role of this pathway is conserved in humans. So far, over 22 different human homolog *CARD9* mutations have been identified that abrogate the Th17 response without affecting total representation of T or B cells (Corvilain et al., 2018), but whether these mutations affect systemic antifungal antibody induction remains unclear. We collected serum from individuals with systemic candidiasis representing non-carriers or carriers of *CARD9* mutations (Q289*, R35Q, R70W; Figure 6I) that have been associated previously with *Candida*-induced meningoencephalitis or colitis (Figure S5E; Lanternier et al., 2015). Individuals with systemic candidiasis mounted a robust antibody response to *C. albicans* (Figures 6I and 6J). In contrast, carriers of mutant *CARD9* alleles produced significantly lower titers of anti-*C. albicans* IgG antibodies (Figures 6I and 6J). These data implicate CARD9 as a critical mediator of systemic anti-fungal IgG antibody responses to the gut commensal *C. albicans* during health and during invasive fungal disease.

DISCUSSION

Although several *Candida* species, including *C. albicans*, are largely regarded as commensals that can evolve and benefit from the intestinal niche (Liang et al., 2019; Tso et al., 2018; Witchley et al., 2019), any benefit to the host from these fungi is still unclear. Our findings outline a model where these gut fungal species play a key role in induction and therapeutic efficacy of host-protective IgG antibodies. The gut mycobiota elicit GC-dependent IgG^{+} B cell expansion through CARD9 signaling in CX3CR1^{+} macrophages to produce antifungal IgG that is protective against systemic fungal infection. Although we did not detect systemic fungal spread, intestinal colonization with *C. albicans*, but not with *S. cerevisiae*, induced a strong IgG CSR in the spleen. CSR was accompanied by transfer of *C. albicans* cell constituents (as assessed by a sensitive DNA-based assay) to this gut-distal organ and was abrogated upon depletion of CX3CR1^{+} MNPs. Furthermore, a previous study has reported that systemic antibodies to specific fungal antigens can arise in mice upon intestinal *C. albicans* colonization (Huertas et al., 2017). These findings suggest that low-grade physiological fungal dissemination, reported previously for other commensals (Macpherson et al., 2000; Zeng et al., 2016), or gut-distal transport of fungal antigens and

PAMPs by migratory phagocytes might play a role in distal induction of systemic anti-fungal antibodies to specific fungal commensals. In humans, we found that loss-of-function mutations in CARD9 that predispose individuals to severe fungal infections are associated with loss of antifungal antibody responses. Immunosuppression, the most common cause of systemic fungal infection in humans (Brown et al., 2012; Koh et al., 2008; Zhai et al., 2020), led to a dramatic decrease in antifungal IgG antibodies in serum of mice associated with rapid gut-to-system *C. albicans* translocation and death, whereas supplementation of systemic antifungal IgG against intestinal *C. albicans* was protective. Furthermore, anti-fungal IgG induced through gastrointestinal colonization was protective against systemic infection with multidrug-resistant *C. auris*, an emerging pathogen for which limited therapies are currently available. Thus, systemic IgG antibodies to the gut mycobiota appear to confer protective antifungal immunity and some degree of cross-specificity (to similar ligands expressed by different fungal species or to cross-reactive ligands) that may be protective against more than one fungal pathogen. Because fungi comprise a widespread kingdom of deadly pathogens for which only a handful of therapies (several antifungal drugs) are clinically available (Fisher et al., 2012; Garcia-Solache and Casadevall, 2010), the pathways activated in the host by the gut mycobiota outlined in our study may warrant further exploration for development of new approaches to antifungal vaccine or neutralizing antibody generation. Furthermore, the human native antifungal antibody pool can be explored for therapeutic purposes in susceptible immunosuppressed individuals, individuals with cancer, and organ transplant recipients or as a potential source of defense against emerging fungal threats.

STAR★METHODS

RESOURCE AVAILABILITY

Lead contact—Further information and requests for resources and reagents should be directed to and will be fulfilled by the Lead Contact, Iliyan D. Iliev (iliev@med.cornell.edu).

Materials availability—This study did not generate new unique reagents.

Data and code availability—All sequencing data are accessible under NCBI archives under the BioProject ID PRJNA630985. All other data needed to evaluate the conclusions in the manuscript are available within the main text or supplementary materials.

EXPERIMENTAL MODEL AND SUBJECT DETAILS

Mice—7–8-week-old wild-type (WT) C57BL/6J, Ighm^{tm1Cgn}/J (μMT$^{-/-}$), Cd11c-cre, Irf4$^{fl/fl}$, Cx3cr$^{1tm\ (DTR)Litt/J}$ (Cx3cr1^{DTR}), Syk $^{fl/fl}$, Cx3cr1$^{tm2.1(cre/ERT2)Jung/J}$ (Cx3cr1-cre/ERT2$^{+/+}$), Tcrb^{tm1Mom}/J, Rag2tm1.1Cgn/J mice were purchased from the Jackson Laboratories (Bar Harbor, ME). Card9$^{-/-}$ mice were kindly provided by Dr. Xin Lin (Department of Molecular and Cellular Oncology, University of Texas, Houston, TX, USA). The Cx3cr1^{DTR} mice were subsequently bred with hemizygous Cd11c-cre$^{+/-}$ mice to allow for selective depletion of CD11c^{+} CD11b^{+} CX3CR1^{+} MNPs upon administration of diphtheria toxin (DT). For depletion, such generated mice (Cd11c-cre$^{+/-}$ Cx3cr1^{DTR} mice) and their respective littermate controls (Cd11c-cre$^{-/-}$ Cx3cr1^{DTR}) were injected for three

consecutive days with 100ng of DT i.p followed by maintenance injection every other day for the length of the experiments. Depleted mice were designated as ΔCX3CR1 mice. $Irf4^{fl/fl}$ mice were bred to hemizygous Cd11c-$cre^{+/-}$ mice to allow for genetic ablation of CD11c $^{+}CD11b^{+}CD103^{+}$ dendritic cells (designated as ΔIrf4 mice) and the generation of littermate controls. $Syk^{fl/fl}$ mice were bred to Cx3cr1-cre/$ERT2^{+/+}$ to allow for the selective depletion of Syk in CX3CR1 expressing cells upon administration of tamoxifen. Cre-ERT recombinase in Cx3cr1-cre/$ERT2^{+/-}$ mice was induced through injection with tamoxifen (TAM, Sigma) that was dissolved in sunflower oil (Sigma) to a final concentration of 10 mg/ml, and 100μl/mouse were injected i.p. every second day. Control littermates received 100 μl sunflower oil i.p every second day. Littermates were randomly assigned to experimental groups. Animals were used between 8 and 16 weeks of age. Males and females were used in approximately equal ratios. Mice were housed under specific pathogen-free (SPF) conditions unless otherwise described at Weill Cornell Medicine and experiments were performed after prior approval by the Institutional Animal Care and Use Committee of Weill Cornell Medicine.

Germ-free (GF) C57BL/6 mouse colonies were maintained within sterile vinyl isolators at Weill Cornell Medicine's gnotobiotic mouse facility. Altered Schaedler Flora (ASF) mice were generated by colonizing GF mice with the defined ASF community (Schaedler et al., 1965) and allowing 5 generations of breeding before use.

Human samples and CARD9 genotyping—Fecal and corresponding serum samples were obtained from healthy de-identified individuals following Institutional-Review-Board-approved protocols from the JRI IBD Live Cell Bank Consortium at Weill Cornell Medicine. Plasma and peripheral blood samples from patients with history of proven invasive candidiasis were collected following informed consent and IRB approval, in accordance with the Helsinki Declaration (Corvilain et al., 2018). DNA samples from human peripheral blood were used for CARD9 genotyping as previously described (Corvilain et al., 2018). Plasma samples from homozygous carriers of either wild-type (n = *5*) or loss of function (n = *4*) *CARD9* alleles were processed for serological evaluation performed by ELISA as described below.

Fungal strains—Fungal strains were obtained from the American Type Culture Collection (Manassas, VA). *Candida albicans* SC5314 (ATCC® MYA-2876) and *Saccharomyces cerevisiae* (ATCC® MYA-796) were cultured in aerobic conditions on Sabouraud Dextrose Broth (SDB; EMD Chemicals) at 37°C overnight, while *Cladosporium cladosporioides* (ATCC® 38810) and *C. auris* (CDC0389) were cultured in SD agar at 30°C for 5–7 days and 24 h, respectively. *Malassezia restricta* (ATCC® MYA-4611) was plated on Dixon agar (HiMedia Laboratories) coated with 2–3 mL of olive oil and grown at 30°C for 3–5 days.

METHOD DETAILS

Multi-kingdom antibody profiling (multiKAP)—For multiKAP, fecal pellets of 7–8 weeks old mice or human feces were collected. For multiKAP analysis across multiple facilities, samples were collected from age-matched mouse colonies born in our facility (WCM-CE) or from mice raised in Taconic Biosciences (TAC) or the Jackson Laboratory

(JAX) 48–72 h after arriving in our facility. Samples were diluted to 25mg feces/mL in PBS, thoroughly homogenized, and filtered through a 35 μm strainer-capped tube (Falcon, 50mL). Resulting fecal slurries were incubated for 90 min at 30°C with serum from the same mouse or the same human subject diluted at 1:20 (mouse serum) or 1:100 (human serum) in blocking buffer (1% bovine serum albumin (BSA, MP Biomedicals)/0.05% sodium azide (Sigma)). After 30-minutes of blocking with staining buffer (2% BSA/0.05% sodium azide), mouse samples were stained with 1:500 mIgA-PE (Thermofisher) and/or 1:200 mIgG-AF647 (Jackson Immunoresearch) antibodies for 45 min at 4°C. Human samples were stained with 1:200 hIgA-PE (Miltenyi) and/or 1:400 hIgG-AF647 (Southern) antibodies. Stained pellets were further fixed in 4% formalin, followed by staining with 1:1000 SYBR-Green (Invitrogen)/1:500 calcofluor white (Sigma), and total fungal and bacterial content was analyzed by flow cytometry. Size separation was achieved by centrifugation at 900 × g for 10 min. The resulting large (fungal) and small (bacterial) IgA- and/or IgG-stained fractions were used for downstream applications such as flow cytometry analysis and/or sorting and/or DNA isolation. In a variation of the method, size separation was performed as a first step followed by serum incubation and antibody staining as above. For IgG isotype multiKAP assays, samples were stained with mIgG1-FITC (Thermofisher), mIgG2b-FITC (Thermofisher), or mIgG3-FITC (BD Phar-Mingen). To avoid spectral overlap between FITC and Sybr-Green dye when FITC-labeled antibodies were used, DNA staining was performed with propidium iodide (PI; Thermofisher) or DAPI (Thermofisher) as an alternative DNA-binding dyes.

Fungal and bacterial cells sorting, and DNA isolation for multiKAP—Antibody bound (IgG^+IgA^+, IgG^+IgA^-, IgG^-IgA^+) and unbound (IgG^-IgA^-) fungal and bacterial fractions were sorted on FACSAria III (BD Bioscience) with a 100 μm flow cell and processed for DNA isolation and microbiota qPCR and sequencing (see Table S1 for primers).

DNA isolation, fungal, and bacterial quantitative PCR analysis—Sorted antibody-bound and unbound fecal fungal and bacterial fractions, or input feces were treated with lyticase (bacterial fractions were left untreated), followed by DNA isolation using QIAGEN's QIAmp DNA mini kit as in Doron et al. (2019). Fungal and bacterial DNA was quantified in each sample by RT-PCR using fungal 18S and bacterial 16S rDNA-specific primers (Table S1) as in Leonardi et al. (2018) and Li et al. (2018).

Mycobiota library generation, sequencing, and analysis—Fungal ITS1–2 regions in rDNA isolated from sorted antibody-bound or unbound fecal fractions were amplified by PCR using the following primers: ITS1F CTTGGTCATTTAGAGGAAGTAA; ITS2R GCTGCGTTCTTCATCGATGC. Primers were modified to include forward (5′ TCGTCGGCAGCGTCAGATGTGTATAAGAGACAG-[locus-specific sequence]) and reverse (5′ GTCTCGTGGGCTCGGAGATGTGTATAAGAGACAG-[locus-specific sequence]) sequencing adaptors (Table S1). ITS1–2 amplicons were generated with 35 cycles using Invitrogen AccuPrime PCR reagents (Carlsbad, CA). In a second PCR reaction, amplicons from each sample were uniquely indexed using Illumina Nextera XT v2 barcoded primers (San Diego, CA), (Tang et al., 2015). Quality control of all libraries were conducted

by qPCR, DNA 1000 Bioanalyzer (Agilent), and Qubit (Life Technologies) to validate and quantify library construction prior to preparing a paired end flow cell. Clonal bridge amplification (Illumina) was performed using a cBot (Illumina). 2 × 250 bp sequencing-by-synthesis was performed on Illumina MiSeq platform (Illumina).

Raw FASTQ ITS1 sequencing data were enriched for high quality reads by removing both the adaptor sequence by cutadapt v1.4.1 or any reads that lacked the proximal primer sequence. Sequence reads were then quality-trimmed by truncating reads below an average quality score of 20 over a 3 base pair (bp) sliding window and removing reads shorter than 100bp. These enriched high-quality reads were aligned to the Targeted Host Fungi (THF) ITS1 database (Tang et al., 2015) using BLAST v2.2.22 and the pick_otus.py pipeline in the QIIME v1.9.1 wrapper with an identity percentage ≥ 97% for OTU picking. The alignment results were tabulated across all reads using the accession identifier of the ITS reference sequences as surrogate OTUs and using a Perl script. ITS sequencing data are available at NCBI Sequence Read Archive (SRA) under the Bioproject ID PRJNA630985.

Fungal Lysate Preparation—Fungal lysates were prepared by fixing pure fungal cultures in 4% paraformaldehyde (PFA, diluted in PBS) for 60 min. Fungal suspensions were then washed 3 times by pelleting at 900 × g for 2 min, aspirating the supernatant, and resuspending the pellet in molecular-grade water. Fungi were treated with a cycle of 3 × (10 min on dry ice, 10 minutes 75°C). Finally, fungal suspensions were sonicated for 8 cycles of 15sec on/30sec off. Fungal debris was centrifuged at 4000 rpm for 2 minutes, after which lysate-containing supernatant was used for ELISA plate coating.

Antifungal ELISA assay—Antifungal antibody titers in serum were measured by enzyme-linked immunosorbent assay (ELISA). Fungal lysates were coated on a 96-well high-binding polystyrene plates (Corning) after diluting 1:50 in 50mM carbonate-bicarbonate buffer (pH 9.5). *Saccharomyces cerevisiae* mannan (Sigma) or bacterial flagellin from *S. typhimurium* (Invivogen) were coated at 5 μg/well and 0.1 μg/well in carbonate-bicarbonate buffer, respectively. Plates for total IgG measurement were coated with anti-mouse-IgG-IgA-IgM (Sigma) or anti-human Ig (Southern) diluted 1:2000 in coating buffer. Mouse serum was then applied to plates diluted at 1:20 and 1:250 in BSA for antigen-specific and total IgG assays, respectively. Human serum was applied at dilutions of 1:4000 and 1:10000 for antigen-specific and total IgG assays, respectively. Total IgG titers were measured against serial dilution standards of mouse (Bethyl Laboratories) and human (Southern) unconjugated IgG antibodies. Plates were developed using alkaline phosphatase-conjugated anti-mouse or anti-human IgG as previously described (Leonardi et al., 2018). Plates were read at OD 405 nm on a microtiter plate reader (Menlo Park, CA).

Assessment of the adaptive responses to gut fungal colonization—GF mice were orally gavaged with PBS or with 1×10^8 *C. albicans*, *S. cerevisiae*, *M. restricta or* with *C. cladosporioides*. ASF mice were orally gavaged with either PBS (ASF control) or with 1×10^8 *C. albicans* or *S. cerevisiae* yeast cells. Alternatively, cefoperazone (0.4 mg/ml; Sigma) was provided to SPF mice *ad libitum* in drinking water for the length of the colonization experiments followed by 1×10^8 *C. albicans* or *S. cerevisiae* yeast cells colonization via oral gavage. Mice were sacrificed at the described time points for blood,

feces, and organ collection. B cell and T cell compartments were assessed by flow cytometry. Total, fungi-specific or flagellin-specific IgG antibody responses in serum collected at the beginning, during, and at the end of the experiment were assessed by ELISA or used in mutiKAP assays.

Isolation of spleen, mesenteric lymph nodes (mLN), Peyer's patches (PP) and blood lymphocytes—Four to six PP were excised from the ileum of each mouse and placed into Hank's Balanced Salt Solution (HBSS) medium (Thermofisher), supplemented with 2 mM EDTA, and were shaken for 10 min at 37°C, followed washing and by mincing with scissors in a medium consisting of RPMI 1640 (Thermofisher), 5% FBS, 100 IU/ml penicillin and 100 μg/ml streptomycin (Thermofisher) and filtered through a nylon mesh (70μm). Spleens and mLNs were processed similarly and mesh-filtered, after which spleens were each treated with 1 mL of 1x RBC lysis buffer (Biolegend) for 2 min. Processed tissues were once again filtered through mesh, washed twice in PBS, and resuspended in cold PBS supplemented with 2% BSA for antibody staining.

Blood samples were prepared for lymphocyte isolation by transferring 50μL of blood into 1.7mL Eppendorf tubes containing 5μL citrate dextrose solution (ACD; Sigma) and mixed by pipetting to prevent coagulation. Blood samples are then treated with 200μL of 1 × RBC lysis buffer for 5 min, washed, and resuspended in cold PBS supplemented with 2% BSA for antibody staining.

Antibodies, FISH probes and flow cytometry analysis of the host response—Cell suspensions prepared as described above were blocked with CD16/CD32 (Mouse BD Fc Block, 2.4G2, BD Biosciences). For B cell compartment analysis, suspensions were stained with antibodies against CD45 (30-F11, Tonbo), CD4 (GK1.5, eBioscience), CD19 (6D5, Biolegend), IgD (11–26c.2a, Biolegend), IgG (polyclonal, Jackson ImmunoResearch), IgM (II/41, Thermofisher), CD95 (DX2, Biolegend), and GL7 antigen (GL7, Biolegend). Dead cells were excluded with eBioscience Fixable Viability Dye eFluor 455UV (Thermofisher). In phagocyte depletion experiments, suspensions were stained with antibodies against CD45 (30-F11, Tonbo), I-A/I-E a (M5/114.15.2, Biolegend), CD11c (N418, Biolegend), CD11b (M1/70, Thermofisher), CX3CR1 (SA011F11, Biolegend), and CD103 (2E7, Thermofisher). Dead cells were excluded with eBioscience Fixable Viability Dye eFluor 506 (Thermofisher). Bacterial FISH staining was performed with Cy5-labeled EUB338 5'-GCTGCCTCCCGTAGGAGT-3' probe (Integrated DNA Technologies; Table S1). Images were acquired under an inverted Nikon Eclipse Ti microscope (Nikon). Flow cytometry was performed using a LSRFortessa (BD Biosciences) and data were analyzed with FlowJo software (TreeStar).

Systemic candidiasis models and B cell adoptive transfer—Pure cultures of *C. albicans* grown in SDB at 37°C were washed in PBS, resuspended at 5×10^5 yeast cells/mL PBS, and were injected at days 0 and 14 in the tail vein of 5–7 weeks old WT and $\mu MT^{-/-}$ mice (1×10^5 yeast cells/mouse). In rescue experiments splenic B cells from 8-week-old GF mice, *C. albicans*-monocolonized ex-GF or *Aicda*$^{-/-}$ mice were purified by MACS negative sorting (Miltenyi), and adoptively transferred (2×10^7 B cells/mouse) into recipient $\mu MT^{-/-}$ mice two days (day 2) before systemic infection with *C. albicans.* Pure cultures of *C. auris*

grown in SDB at 30°C were washed in PBS, resuspended at 5×10^8 yeast cells/mL PBS, and were injected at days 0 and 14 in the tail vein of 5–7 weeks old WT (1×10^8 yeast cells/mouse). At day 1 and 10 mice received i.p. injection of 400μg *C.aur*-IgG, *C.alb*-IgG, or sterile PBS. Disease progression was tracked for 28 days in all experimental groups. Moribund mice were sacrificed for serum, kidney, and brain tissue collection.

μMT$^{-/-}$ mice were treated for five days with 0.5 mg/ml fluconazole (Sigma), 1 mg/ml Penicillin G (Sigma), and 2 mg/ml streptomycin sulfate (Research Products International) *ad libitum* in the drinking water. Fluconazole was withdrawn and mice were orally gavaged with 1×10^8 *C. albicans* cells. Splenic B cells from 8-week-old *CARD9*$^{+/+}$ or *CARD9*$^{-/-}$ mice were purified by MACS negative sorting (Miltenyi), and adoptively transferred (2×10^7 B cells/mouse) into recipient μMT$^{-/-}$ mice one day after the intestinal colonization with *C. albicans.* Serum was collected weekly; mice were sacrificed at 4 weeks for intestinal tissue and spleen collection.

Serum IgG purification from monocolonized ex-GF mice—GF were weaned after 4 weeks and orally gavaged with 1×10^8 *C. albicans, C. auris* or *S. cerevisiae* cells cultured from pure isolates overnight at 37°C. Between ages of 8–12 weeks, blood was collected every 3 days from each respective group and pooled. After 1 h of room temperature incubation to allow for coagulation the blood was centrifuged for 10 min at 6000 × g. The top layer of serum was transferred to a separate Eppendorf tube and stored at −20°C until purification. IgG was purified from pooled serum using the Protein G UltraLink™ Columns (Pierce). Purified IgG samples were desalted through buffer exchange to PBS using Amicon®Ultra-15 Centrifugal Filter tubes (Millipore). After measuring the IgG concentration and assessing specificity, pure IgG suspensions (*C.alb*-IgG, *C.aur*-IgG or *S.cer*-IgG) were adjusted with cold sterile PBS to 4 mg/mL and stored at −20°C until use. Pure IgG suspensions were delivered intraperitoneally for a single dose of 400μg IgG.

Gut-disseminating candidiasis model—Mice were treated for five days with 0.5 mg/ml fluconazole (Sigma), 1 mg/ml Penicillin G (Sigma), and 2 mg/ml streptomycin sulfate (Research Products International) *ad libitum* in the drinking water. Fluconazole was withdrawn and mice were orally gavaged with 1×10^8 *C. albicans* cells three times spaced across five days, followed by i.p. injection of 400μg *C.alb*-IgG, *S.cer*-IgG, or sterile PBS (Figure S4B). Immunosuppression and systemic fungal dissemination were induced by i.p. injections of 150mg/kg mouse weight of cyclophosphamide (Cyc; R&D Systems) on days 0, 2, and 4, followed by a second series of injections on days 14, 16, and 18. Weight was measured, and moribund mice were sacrificed for serum, liver, and kidney tissue collection.

Single-cell RNA seq analysis—To assess the expression of CARD9 among immune cells in humans we mined a published single-cell RNA sequencing (scRNA-seq) dataset obtained from colon biopsies from healthy individuals in (Smillie et al., 2019). Plots were created using the published differentially expressed genes for cell subsets, lineages, or sub-clusters in healthy tissue, relative to all other cells. These sequencing data are accessible under the Single Cell Portal (https://singlecell.broadinstitute.org/single_cell) under the Accession Number SCP259.

QUANTIFICATION AND STATISTICAL ANALYSIS

Statistics were computed using GraphPad Prism version 8 (GraphPad Software) using the Mann-Whitney test (which does not assume normal distribution) for two groups. One-way ANOVA with Tukey's or Kruskal-Wallis and Dunn's for multiple comparisons was used for three or more groups. Statistical details specific to experiments are reported in the figure legends. Graphs display mean values with error bars that correspond to the standard error of the mean (mean ± SEM). The p value(s) reported in the figure legends are the likelihood(s) of observing the effect size(s), if the null hypothesis of zero difference is true. They are denoted as: not significant (ns) $p \geq 0.05$, *$p < 0.05$, **$p < 0.01$, ***$p < 0.001$, ****$p < 0.0001$.

ITS1 Sequencing Analysis of FACS-sorted mycobiota—Relative abundances at the species level were analyzed by R (v3.4.4) with the Phyloseq (1.22.3) and Vegan (2.5–3) packages. Species representing less than 2% of total reads among all samples were grouped into the "Other" category. Sorted populations from one individual were excluded due to contamination. For each species, the coating index (CI) was calculated using previously determined (Kau et al., 2015), shown in Figure S2C. Enrichment in antibody-bound or antibody-unbound populations was tested for each species by one-sample t test in GraphPad Prism (GraphPad Software) to determine whether mean CI values deviated significantly from 0.

Supplementary Material

Refer to Web version on PubMed Central for supplementary material.

ACKNOWLEDGMENTS

We thank members of the Iliev laboratory for critical review of the manuscript. We thank Jean-Laurent Casanova of the Laboratory of Human Genetics of Infectious Diseases at Rockefeller University and Howard Hughes Medical Institute for help with the human genetics study of CARD9. We thank Jayanta Chaudhuri and Tobias Hohl for discussions and for providing a key reagent. We thank all contributing members of the JRI IBD Live Cell Bank Consortium and the Microbiome Core Laboratory of Weill Cornell Medicine. Support for sample acquisition through the JRI IBD Live Cell Bank is provided by the JRI, the Jill Roberts Center for IBD, Cure for IBD, the Rosanne H. Silbermann Foundation, and the Weill Cornell Medicine Division of Pediatric Gastroenterology and Nutrition. Research in the Iliev laboratory is supported by the National Institutes of Health (DK113136, DK121977, and AI137157), the Leona M. and Harry B. Helmsley Charitable Trust, the Crohn's and Colitis Foundation, the Irma T. Hirschl Career Scientist Award, pilot project funding from the Center for Advanced Digestive Care (CADC), the Jill Roberts Institute (JRI) for Research in IBD, and the Burroughs Wellcome Fund Investigator in the Pathogenesis of Infectious Diseases Award.

REFERENCES

Ansaldo E, Slayden LC, Ching KL, Koch MA, Wolf NK, Plichta DR, Brown EM, Graham DB, Xavier RJ, Moon JJ, and Barton GM (2019). *Akkermansia muciniphila* induces intestinal adaptive immune responses during homeostasis. Science 364, 1179–1184. [PubMed: 31221858]

Arumugam M, Raes J, Pelletier E, Le Paslier D, Yamada T, Mende DR, Fernandes GR, Tap J, Bruls T, Batto J-M, et al.; MetaHIT Consortium (2011). Enterotypes of the human gut microbiome. Nature 473, 174–180. [PubMed: 21508958]

Bacher P, Hohnstein T, Beerbaum E, Röcker M, Blango MG, Kaufmann S, Röhmel J, Eschenhagen P, Grehn C, Seidel K, et al. (2019). Human Anti-fungal Th17 Immunity and Pathology Rely on Cross-Reactivity against Candida albicans. Cell 176, 1340–1355.e15. [PubMed: 30799037]

Barbet G, Sander LE, Geswell M, Leonardi I, Cerutti A, Iliev I, and Blander JM (2018). Sensing Microbial Viability through Bacterial RNA Augments T Follicular Helper Cell and Antibody Responses. Immunity 48, 584–598.e5. [PubMed: 29548673]

Brown GD, Denning DW, Gow NAR, Levitz SM, Netea MG, and White TC (2012). Hidden killers: human fungal infections. Sci. Transl. Med 4, 165rv13.

Bunker JJ, Flynn TM, Koval JC, Shaw DG, Meisel M, McDonald BD, Ishizuka IE, Dent AL, Wilson PC, Jabri B, et al. (2015). Innate and Adaptive Humoral Responses Coat Distinct Commensal Bacteria with Immunoglobulin A. Immunity 43, 541–553. [PubMed: 26320660]

Cao Z, Conway KL, Heath RJ, Rush JS, Leshchiner ES, Ramirez-Ortiz ZG, Nedelsky NB, Huang H, Ng A, Gardet A, et al. (2015). Ubiquitin Ligase TRIM62 Regulates CARD9-Mediated Anti-fungal Immunity and Intestinal Inflammation. Immunity 43, 715–726. [PubMed: 26488816]

Casadevall A, and Pirofski L-A (2003). Exploiting the redundancy in the immune system: vaccines can mediate protection by eliciting ‘unnatural’ immunity. J. Exp. Med 197, 1401–1404. [PubMed: 12782708]

Casadevall A, and Pirofski LA (2012). Immunoglobulins in defense, pathogenesis, and therapy of fungal diseases. Cell Host Microbe 11, 447–456. [PubMed: 22607798]

Chiani P, Bromuro C, Cassone A, and Torosantucci A (2009). Anti-β-glucan antibodies in healthy human subjects. Vaccine 27, 513–519. [PubMed: 19041357]

Christmann BS, Abrahamsson TR, Bernstein CN, Duck LW, Mannon PJ, Berg G, Björkstén B, Jenmalm MC, and Elson CO (2015). Human seroreactivity to gut microbiota antigens. J. Allergy Clin. Immunol 136, 1378–86.e1, 5. [PubMed: 26014812]

Conti HR, Shen F, Nayyar N, Stocum E, Sun JN, Lindemann MJ, Ho AW, Hai JH, Yu JJ, Jung JW, et al. (2009). Th17 cells and IL-17 receptor signaling are essential for mucosal host defense against oral candidiasis. J. Exp. Med 206, 299–311. [PubMed: 19204111]

Corvilain E, Casanova J-L, and Puel A (2018). Inherited CARD9 Deficiency: Invasive Disease Caused by Ascomycete Fungi in Previously Healthy Children and Adults. J. Clin. Immunol 38, 656–693. [PubMed: 30136218]

Daims H, Brühl A, Amann R, Schleifer KH, and Wagner M (1999). The domain-specific probe EUB338 is insufficient for the detection of all Bacteria: development and evaluation of a more comprehensive probe set. Syst. Appl. Microbiol 22, 434–444. [PubMed: 10553296]

Doron I, Leonardi I, and Iliev ID (2019). Profound mycobiome differences between segregated mouse colonies do not influence Th17 responses to a newly introduced gut fungal commensal. Fungal Genet. Biol 127, 45–49. [PubMed: 30849443]

Drummond RA, Collar AL, Swamydas M, Rodriguez CA, Lim JK, Mendez LM, Fink DL, Hsu AP, Zhai B, Karauzum H, et al. (2015). CARD9-Dependent Neutrophil Recruitment Protects against Fungal Invasion of the Central Nervous System. PLoS Pathog. 11, e1005293. [PubMed: 26679537]

Edwards JE Jr., Schwartz MM, Schmidt CS, Sobel JD, Nyirjesy P, Schodel F, Marchus E, Lizakowski M, DeMontigny EA, Hoeg J, et al. (2018). A Fungal Immunotherapeutic Vaccine (NDV-3A) for Treatment of Recurrent Vulvovaginal Candidiasis-A Phase 2 Randomized, Double-Blind, Placebo-Controlled Trial. Clin. Infect. Dis 66, 1928–1936. [PubMed: 29697768]

Evans DM, Spencer CCA, Pointon JJ, Su Z, Harvey D, Kochan G, Oppermann U, Dilthey A, Pirinen M, Stone MA, et al.; Spondyloarthritis Research Consortium of Canada (SPARCC); Australo-Anglo-American Spondyloarthritis Consortium (TASC); Wellcome Trust Case Control Consortium 2 (WTCCC2) (2011). Interaction between ERAP1 and HLA-B27 in ankylosing spondylitis implicates peptide handling in the mechanism for HLA-B27 in disease susceptibility. Nat. Genet 43, 761–767. [PubMed: 21743469]

Eyre DW, Sheppard AE, Madder H, Moir I, Moroney R, Quan TP, Griffiths D, George S, Butcher L, Morgan M, et al. (2018). A Candida auris Outbreak and Its Control in an Intensive Care Setting. N. Engl. J. Med 379, 1322–1331. [PubMed: 30281988]

Fadlallah J, Sterlin D, Fieschi C, Parizot C, Dorgham K, El Kafsi H, Autaa G, Ghillani-Dalbin P, Juste C, Lepage P, et al. (2019). Synergistic convergence of microbiota-specific systemic IgG and secretory IgA. J. Allergy Clin. Immunol 143, 1575–1585.e4. [PubMed: 30554723]

Fan D, Coughlin LA, Neubauer MM, Kim J, Kim MS, Zhan X, Simms-Waldrip TR, Xie Y, Hooper LV, and Koh AY (2015). Activation of HIF-1α and LL-37 by commensal bacteria inhibits Candida albicans colonization. Nat. Med 21, 808–814. [PubMed: 26053625]

Fisher MC, Henk DA, Briggs CJ, Brownstein JS, Madoff LC, McCraw SL, and Gurr SJ (2012). Emerging fungal threats to animal, plant and ecosystem health. Nature 484, 186–194. [PubMed: 22498624]

Flores-Langarica A, Cook C, Müller Luda K, Persson EK, Marshall JL, Beristain-Covarrubias N, Yam-Puc JC, Dahlgren M, Persson JJ, Uematsu S, et al. (2018). Intestinal $CD103^{+}CD11b^{+}$ cDC2 Conventional Dendritic Cells Are Required for Primary $CD4^{+}$ T and B Cell Responses to Soluble Flagellin. Front. Immunol 9, 2409. [PubMed: 30386346]

Garcia-Solache MA, and Casadevall A (2010). Global warming will bring new fungal diseases for mammals. MBio 1, e00061–10. [PubMed: 20689745]

Glocker E-O, Hennigs A, Nabavi M, Schäffer AA, Woellner C, Salzer U, Pfeifer D, Veelken H, Warnatz K, Tahami F, et al. (2009). A homozygous CARD9 mutation in a family with susceptibility to fungal infections. N. Engl. J. Med 361, 1727–1735. [PubMed: 19864672]

Hand TW, Dos Santos LM, Bouladoux N, Molloy MJ, Pagán AJ, Pepper M, Maynard CL, Elson CO 3rd, and Belkaid Y (2012). Acute gastro-intestinal infection induces long-lived microbiota-specific T cell responses. Science 337, 1553–1556. [PubMed: 22923434]

Hsu Y-MS, Zhang Y, You Y, Wang D, Li H, Duramad O, Qin X-F, Dong C, and Lin X (2007). The adaptor protein CARD9 is required for innate immune responses to intracellular pathogens. Nat. Immunol 8, 198–205. [PubMed: 17187069]

Huertas B, Prieto D, Pitarch A, Gil C, Pla J, and Díez-Orejas R (2017). Serum Antibody Profile during Colonization of the Mouse Gut by Candida albicans: Relevance for Protection during Systemic Infection. J. Proteome Res 16, 335–345. [PubMed: 27539120]

Jostins L, Ripke S, Weersma RK, Duerr RH, McGovern DP, Hui KY, Lee JC, Schumm LP, Sharma Y, Anderson CA, et al.; International IBD Genetics Consortium (IIBDGC) (2012). Host-microbe interactions have shaped the genetic architecture of inflammatory bowel disease. Nature 491, 119–124. [PubMed: 23128233]

Kau AL, Planer JD, Liu J, Rao S, Yatsunenko T, Trehan I, Manary MJ, Liu T-C, Stappenbeck TS, Maleta KM, et al. (2015). Functional characterization of IgA-targeted bacterial taxa from undernourished Malawian children that produce diet-dependent enteropathy. Sci. Transl. Med 7, 276ra24.

Kim Y-I, Song J-H, Ko H-J, Kweon M-N, Kang C-Y, Reinecker H-C, and Chang S-Y (2018). CX_3CR1^{+} Macrophages and $CD8^{+}$ T Cells Control Intestinal IgA Production. J. Immunol 201, 1287–1294. [PubMed: 29987162]

Kim SG, Becattini S, Moody TU, Shliaha PV, Littmann ER, Seok R, Gjonbalaj M, Eaton V, Fontana E, Amoretti L, et al. (2019). Microbiota-derived lantibiotic restores resistance against vancomycin-resistant Enterococcus. Nature 572, 665–669. [PubMed: 31435014]

Koch MA, Reiner GL, Lugo KA, Kreuk LS, Stanbery AG, Ansaldo E, Seher TD, Ludington WB, and Barton GM (2016). Maternal IgG and IgA Antibodies Dampen Mucosal T Helper Cell Responses in Early Life. Cell 165, 827–841. [PubMed: 27153495]

Koh AY, Köhler JR, Coggshall KT, Van Rooijen N, and Pier GB (2008). Mucosal damage and neutropenia are required for Candida albicans dissemination. PLoS Pathog. 4, e35. [PubMed: 18282097]

Koscsó B, Kurapati S, Rodrigues RR, Nedjic J, Gowda K, Shin C, Soni C, Ashraf AZ, Purushothaman I, Palisoc M, et al. (2020). Gut-resident $CX3CR1^{hi}$ macrophages induce tertiary lymphoid structures and IgA response in situ. Sci. Immunol 5, eaax0062. [PubMed: 32276965]

Lamas B, Richard ML, Leducq V, Pham H-P, Michel M-L, Da Costa G, Bridonneau C, Jegou S, Hoffmann TW, Natividad JM, et al. (2016). CARD9 impacts colitis by altering gut microbiota metabolism of tryptophan into aryl hydrocarbon receptor ligands. Nat. Med 22, 598–605. [PubMed: 27158904]

Lanternier F, Mahdaviani SA, Barbati E, Chaussade H, Koumar Y, Levy R, Denis B, Brunel AS, Martin S, Loop M, et al. (2015). Inherited CARD9 deficiency in otherwise healthy children and

adults with Candida species-induced meningoencephalitis, colitis, or both. J. Allergy Clin. Immunol 135, 1558–1568.e2. [PubMed: 25702837]

LeibundGut-Landmann S, Gross O, Robinson MJ, Osorio F, Slack EC, Tsoni SV, Schweighoffer E, Tybulewicz V, Brown GD, Ruland J, and Reis e Sousa C (2007). Syk- and CARD9-dependent coupling of innate immunity to the induction of T helper cells that produce interleukin 17. Nat. Immunol 8, 630–638. [PubMed: 17450144]

Leonardi I, Li X, Semon A, Li D, Doron I, Putzel G, Bar A, Prieto D, Rescigno M, McGovern DPB, et al. (2018). CX3CR1^{+} mononuclear phagocytes control immunity to intestinal fungi. Science 359, 232–236. [PubMed: 29326275]

Leonardi I, Paramsothy S, Doron I, Semon A, Kaakoush NO, Clemente JC, Faith JJ, Borody TJ, Mitchell HM, Colombel JF, et al. (2020). Fungal Trans-kingdom Dynamics Linked to Responsiveness to Fecal Microbiota Transplantation (FMT) Therapy in Ulcerative Colitis. Cell Host Microbe 27, 823–829.e3. [PubMed: 32298656]

Li X, Leonardi I, Semon A, Doron I, Gao IH, Putzel GG, Kim Y, Kabata H, Artis D, Fiers WD, et al. (2018). Response to Fungal Dysbiosis by Gut-Resident CX3CR1^{+} Mononuclear Phagocytes Aggravates Allergic Airway Disease. Cell Host Microbe 24, 847–856.e4. [PubMed: 30503509]

Li XV, Leonardi I, and Iliev ID (2019). Gut Mycobiota in Immunity and Inflammatory Disease. Immunity 50, 1365–1379. [PubMed: 31216461]

Liang S-H, Anderson MZ, Hirakawa MP, Wang JM, Frazer C, Alaalm LM, Thomson GJ, Ene IV, and Bennett RJ (2019). Hemizygosity Enables a Mutational Transition Governing Fungal Virulence and Commensalism. Cell Host Microbe 25, 418–431.e6. [PubMed: 30824263]

Lionakis MS, Netea MG, and Holland SM (2014). Mendelian genetics of human susceptibility to fungal infection. Cold Spring Harb. Perspect. Med 4, a019638. [PubMed: 24890837]

Liu CM, Kachur S, Dwan MG, Abraham AG, Aziz M, Hsueh PR, Huang YT, Busch JD, Lamit LJ, Gehring CA, et al. (2012). FungiQuant: a broad-coverage fungal quantitative real-time PCR assay. BMC Microbiol. 12, 255. [PubMed: 23136846]

Macpherson AJ, Gatto D, Sainsbury E, Harriman GR, Hengartner H, and Zinkernagel RM (2000). A primitive T cell-independent mechanism of intestinal mucosal IgA responses to commensal bacteria. Science 288, 2222–2226. [PubMed: 10864873]

Martinez LR, Moussai D, and Casadevall A (2004). Antibody to *Cryptococcus neoformans* glucuronoxylomannan inhibits the release of capsular antigen. Infect. Immun 72, 3674–3679. [PubMed: 15155683]

McClelland EE, Nicola AM, Prados-Rosales R, and Casadevall A (2010). Ab binding alters gene expression in Cryptococcus neoformans and directly modulates fungal metabolism. J. Clin. Invest 120, 1355–1361. [PubMed: 20335660]

Montagnoli C, Bozza S, Bacci A, Gaziano R, Mosci P, Morschhäuser J, Pitzurra L, Kopf M, Cutler J, and Romani L (2003). A role for antibodies in the generation of memory antifungal immunity. Eur. J. Immunol 33, 1193–1204. [PubMed: 12731044]

Moreno-Sabater A, Autaa G, Sterlin D, Jerbi A, Villette R, Holm JB, Parizot C, Selim S, Senghor Y, Ghillani-Dalbin P, et al. (2020). Systemic anti-commensal response to fungi analyzed by flow cytometry is related to gut mycobiome ecology. Microbiome 8, 159. [PubMed: 33190643]

Nash AK, Auchtung TA, Wong MC, Smith DP, Gesell JR, Ross MC, Stewart CJ, Metcalf GA, Muzny DM, Gibbs RA, et al. (2017). The gut mycobiome of the Human Microbiome Project healthy cohort. Microbiome 5, 153. [PubMed: 29178920]

Pachl J, Svoboda P, Jacobs F, Vandewoude K, van der Hoven B, Spronk P, Masterson G, Malbrain M, Aoun M, Garbino J, et al.; Mycograb Invasive Candidiasis Study Group (2006). A randomized, blinded, multi-center trial of lipid-associated amphotericin B alone versus in combination with an antibody-based inhibitor of heat shock protein 90 in patients with invasive candidiasis. Clin. Infect. Dis 42, 1404–1413. [PubMed: 16619152]

Palm NW, de Zoete MR, Cullen TW, Barry NA, Stefanowski J, Hao L, Degnan PH, Hu J, Peter I, Zhang W, et al. (2014). Immunoglobulin A coating identifies colitogenic bacteria in inflammatory bowel disease. Cell 158, 1000–1010. [PubMed: 25171403]

Pérez de Diego R, Sánchez-Ramón S, López-Collazo E, Martínez-Barricarte R, Cubillos-Zapata C, Ferreira Cerdán A, Casanova J-L, and Puel A (2015). Genetic errors of the human caspase

recruitment domain-B-cell lymphoma 10-mucosa-associated lymphoid tissue lymphoma-translocation gene 1 (CBM) complex: Molecular, immunologic, and clinical heterogeneity. J. Allergy Clin. Immunol 136, 1139–1149. [PubMed: 26277595]

Plotkin SA (2010). Correlates of protection induced by vaccination. Clin. Vaccine Immunol 17, 1055–1065. [PubMed: 20463105]

Rapaka RR, Ricks DM, Alcorn JF, Chen K, Khader SA, Zheng M, Plevy S, Bengtén E, and Kolls JK (2010). Conserved natural IgM antibodies mediate innate and adaptive immunity against the opportunistic fungus Pneumocystis murina. J. Exp. Med 207, 2907–2919. [PubMed: 21149550]

Richard ML, and Sokol H (2019). The gut mycobiota: insights into analysis, environmental interactions and role in gastrointestinal diseases. Nat. Rev. Gastroenterol. Hepatol 16, 331–345. [PubMed: 30824884]

Riente L, Chimenti D, Pratesi F, Delle Sedie A, Tommasi S, Tommasi C, Bombardieri S, and Migliorini P (2004). Antibodies to tissue transglutaminase and Saccharomyces cerevisiae in ankylosing spondylitis and psoriatic arthritis. J. Rheumatol 31, 920–924. [PubMed: 15124251]

Rivas MA, Beaudoin M, Gardet A, Stevens C, Sharma Y, Zhang CK, Boucher G, Ripke S, Ellinghaus D, Burtt N, et al.; National Institute of Diabetes and Digestive Kidney Diseases Inflammatory Bowel Disease Genetics Consortium (NIDDK IBDGC); United Kingdom Inflammatory Bowel Disease Genetics Consortium; International Inflammatory Bowel Disease Genetics Consortium (2011). Deep resequencing of GWAS loci identifies independent rare variants associated with inflammatory bowel disease. Nat. Genet 43, 1066–1073. [PubMed: 21983784]

Roth S, and Ruland J (2013). Caspase recruitment domain-containing protein 9 signaling in innate immunity and inflammation. Trends Immunol. 34, 243–250. [PubMed: 23523010]

Rudkin FM, Raziunaite I, Workman H, Essono S, Belmonte R, MacCallum DM, Johnson EM, Silva LM, Palma AS, Feizi T, et al. (2018). Single human B cell-derived monoclonal anti-Candida antibodies enhance phagocytosis and protect against disseminated candidiasis. Nat. Commun 9, 5288. [PubMed: 30538246]

Schaedler RW, Dubos R, and Costello R (1965). The development of the bacterial flora in the gastrointestinal tract of mice. J. Exp. Med 122, 59–66. [PubMed: 14325473]

Shao T-Y, Ang WXG, Jiang TT, Huang FS, Andersen H, Kinder JM, Pham G, Burg AR, Ruff B, Gonzalez T, et al. (2019). Commensal Candida albicans Positively Calibrates Systemic Th17 Immunological Responses. Cell Host Microbe 25, 404–417.e6. [PubMed: 30870622]

Slack E, Hapfelmeier S, Stecher B, Velykoredko Y, Stoel M, Lawson MAE, Geuking MB, Beutler B, Tedder TF, Hardt W-D, et al. (2009). Innate and adaptive immunity cooperate flexibly to maintain host-microbiota mutualism. Science 325, 617–620. [PubMed: 19644121]

Smillie CS, Biton M, Ordovas-Montanes J, Sullivan KM, Burgin G, Graham DB, Herbst RH, Rogel N, Slyper M, Waldman J, et al. (2019). Intra- and Inter-cellular Rewiring of the Human Colon during Ulcerative Colitis. Cell 178, 714–730.e22. [PubMed: 31348891]

Sokol H, Leducq V, Aschard H, Pham H-P, Jegou S, Landman C, Cohen D, Liguori G, Bourrier A, Nion-Larmurier I, et al. (2017). Fungal microbiota dysbiosis in IBD. Gut 66, 1039–1048. [PubMed: 26843508]

Standaert-Vitse A, Jouault T, Vandewalle P, Mille C, Seddik M, Sendid B, Mallet JM, Colombel JF, and Poulain D (2006). Candida albicans is an immunogen for anti-Saccharomyces cerevisiae antibody markers of Crohn's disease. Gastroenterology 130, 1764–1775. [PubMed: 16697740]

Standaert-Vitse A, Sendid B, Joossens M, François N, Vandewalle-El Khoury P, Branche J, Van Kruiningen H, Jouault T, Rutgeerts P, Gower-Rousseau C, et al. (2009). Candida albicans colonization and ASCA in familial Crohn's disease. Am. J. Gastroenterol 104, 1745–1753. [PubMed: 19471251]

Takaki H, Kure S, Oshiumi H, Sakoda Y, Suzuki T, Ainai A, Hasegawa H, Matsumoto M, and Seya T (2018). Toll-like receptor 3 in nasal $CD103^{+}$ dendritic cells is involved in immunoglobulin A production. Mucosal Immunol. 11, 82–96. [PubMed: 28612840]

Tang J, Iliev ID, Brown J, Underhill DM, and Funari VA (2015). Mycobiome: Approaches to analysis of intestinal fungi. J. Immunol. Methods 421, 112–121. [PubMed: 25891793]

Teng F, Klinger CN, Felix KM, Bradley CP, Wu E, Tran NL, Umesaki Y, and Wu HJ (2016). Gut Microbiota Drive Autoimmune Arthritis by Promoting Differentiation and Migration of Peyer's Patch T Follicular Helper Cells. Immunity 44, 875–888. [PubMed: 27096318]

Tso GHW, Reales-Calderon JA, Tan ASM, Sem X, Le GTT, Tan TG, Lai GC, Srinivasan KG, Yurieva M, Liao W, et al. (2018). Experimental evolution of a fungal pathogen into a gut symbiont. Science 362, 589–595. [PubMed: 30385579]

Victora GD, and Nussenzweig MC (2012). Germinal centers. Annu. Rev. Immunol 30, 429–457. [PubMed: 22224772]

Witchley JN, Penumetcha P, Abon NV, Woolford CA, Mitchell AP, and Noble SM (2019). Candida albicans Morphogenesis Programs Control the Balance between Gut Commensalism and Invasive Infection. Cell Host Microbe 25, 432–443.e6. [PubMed: 30870623]

Wüthrich M, Deepe GS Jr., and Klein B (2012). Adaptive immunity to fungi. Annu. Rev. Immunol 30, 115–148. [PubMed: 22224780]

Yang A-M, Inamine T, Hochrath K, Chen P, Wang L, Llorente C, Bluemel S, Hartmann P, Xu J, Koyama Y, et al. (2017). Intestinal fungi contribute to development of alcoholic liver disease. J. Clin. Invest 127, 2829–2841. [PubMed: 28530644]

Zeng MY, Cisalpino D, Varadarajan S, Hellman J, Warren HS, Cascalho M, Inohara N, and Núñez G (2016). Gut Microbiota-Induced Immuno-globulin G Controls Systemic Infection by Symbiotic Bacteria and Pathogens. Immunity 44, 647–658. [PubMed: 26944199]

Zhai B, Ola M, Rolling T, Tosini NL, Joshowitz S, Littmann ER, Amoretti LA, Fontana E, Wright RJ, Miranda E, et al. (2020). High-resolution mycobiota analysis reveals dynamic intestinal translocation preceding invasive candidiasis. Nat. Med 26, 59–64. [PubMed: 31907459]

Highlights

- Multi-kingdom antibody profiling reveled systemic IgG repertoires against gut fungi
- *Candida albicans* is the major inducer of antifungal IgG (αF-IgG) in mice and humans
- Gut-induced anti-*Candida* IgG protects against systemic *C. albicans* and *C. auris*
- $CARD9^{+}CX3CR1^{+}$ phagocytes mediate αF-IgG that is decreased in CARD9-deficient patients

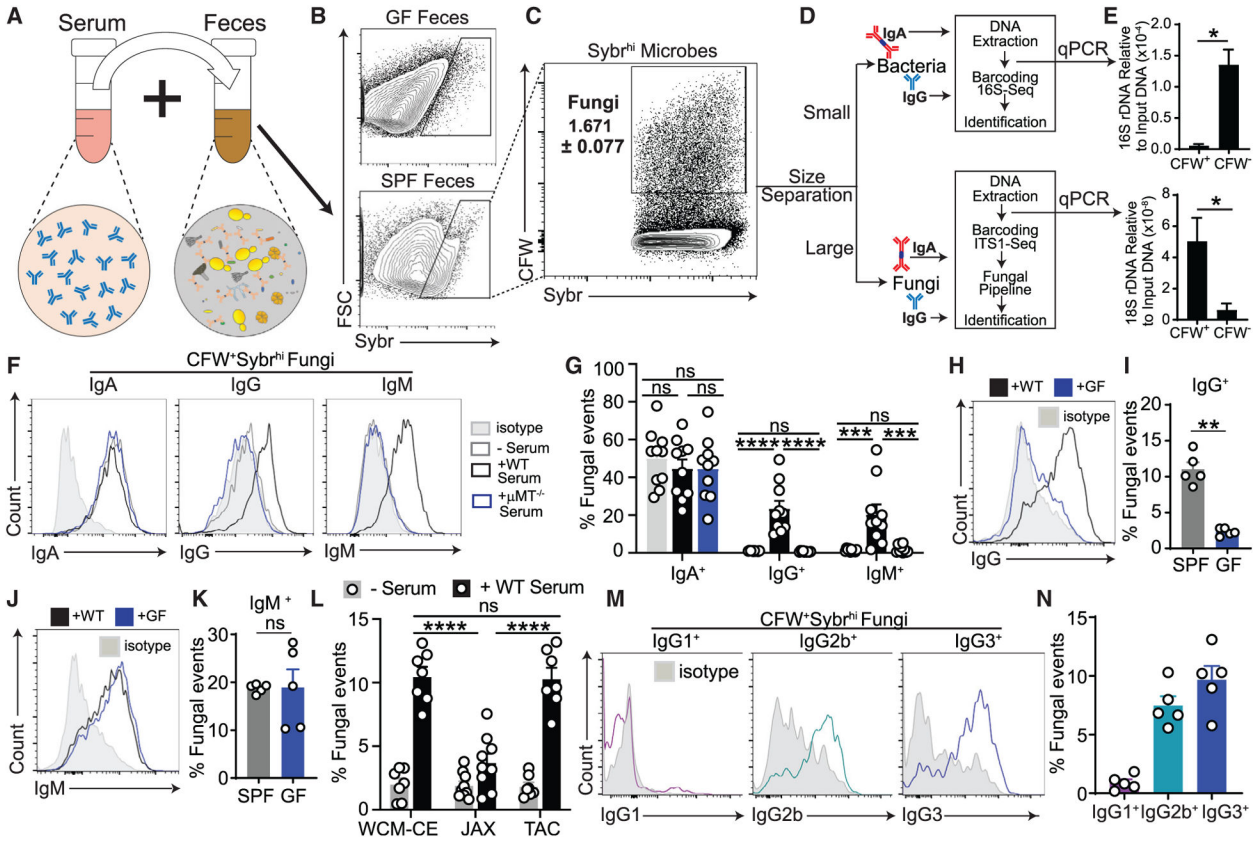

Figure 1. Systemic IgG antibodies bind gut mycobiota

(A–E) MultiKAP assay. Serum and feces are co-incubated to allow serum IgG to bind to gut microbial epitopes.

(A and B) Fecal microbes are distinguished as a Sybr^{hi} population that is absent in similarly stained GF feces (B).

(C) Antibody-reactive microbiota (fungi and bacteria) analysis is performed by flow cytometry, and then fungi (Sybr^{hi}CFW^{+}) and bacteria (Sybr^{hi}CFW^{+}) are enriched in two respective fractions (large and small) through size separation by 900 × *g* centrifugation.

(D) Antibody-bound fungi and bacteria from each sample are sorted by fluorescence-activated cell sorting (FACS), and DNA is isolated and used in downstream applications such as PCR-based quantification and fungal (ITS1) and bacterial (16S) analysis through amplicon-based deep-sequencing.

(E) Quantitative PCR-based assessment of the enriched fungal or bacterial population; Mann-Whitney test. CFW^{+}, n = 4; CFW^{-}, n = 4.

(F and G) Fungi in SPF mouse feces were assessed for IgA, IgG, and IgM binding by multiKAP; no serum incubation (gray), incubation with matched WT SPF mouse serum (black), or B cell-deficient *μMT*$^{-/-}$ SPF mouse serum (blue). Pooled from two independent experiments; one-way ANOVA followed by Tukey's multiple comparisons test. −Serum, n = 10; +WT serum, n = 10; +*μMT*$^{-/-}$ serum, n = 10.

(H–K) Fungi in WT SPF mouse feces were assessed for IgG (H and I) and IgM binding (J and K) by multiKAP after incubation with matched WT SPF (black) or WT GF (blue) serum. Mann-Whitney test. SPF, n = 5; GF, n = 5.

(L) MultiKAP assay with feces from mice from a dedicated controlled environment room at Weill Cornell Medicine (WCM-CE) and Jackson Laboratory (JAX) or Taconic Bioscience (TAC) facilities with (+serum) or without (−serum) serum co-incubation. Pooled from two independent experiments; one-way ANOVA followed by Tukey's multiple comparisons test. WCM-CE, n = 7; JAX, n = 9; TAC, n = 7.

(M and N) Fungi in SPF WT mouse feces were assessed for IgG1, IgG2b, and IgG3 binding by multiKAP after incubation with matched WT SPF serum. IgG1, n = 5; IgG2b, n = 5; IgG3, n = 5.

Error bars indicate SEM. ns, $p \geq 0.05$; *$p < 0.05$; **$p < 0.01$; ***$p < 0.001$; ****$p < 0.0001$. See also Figure S1 and Table S1.

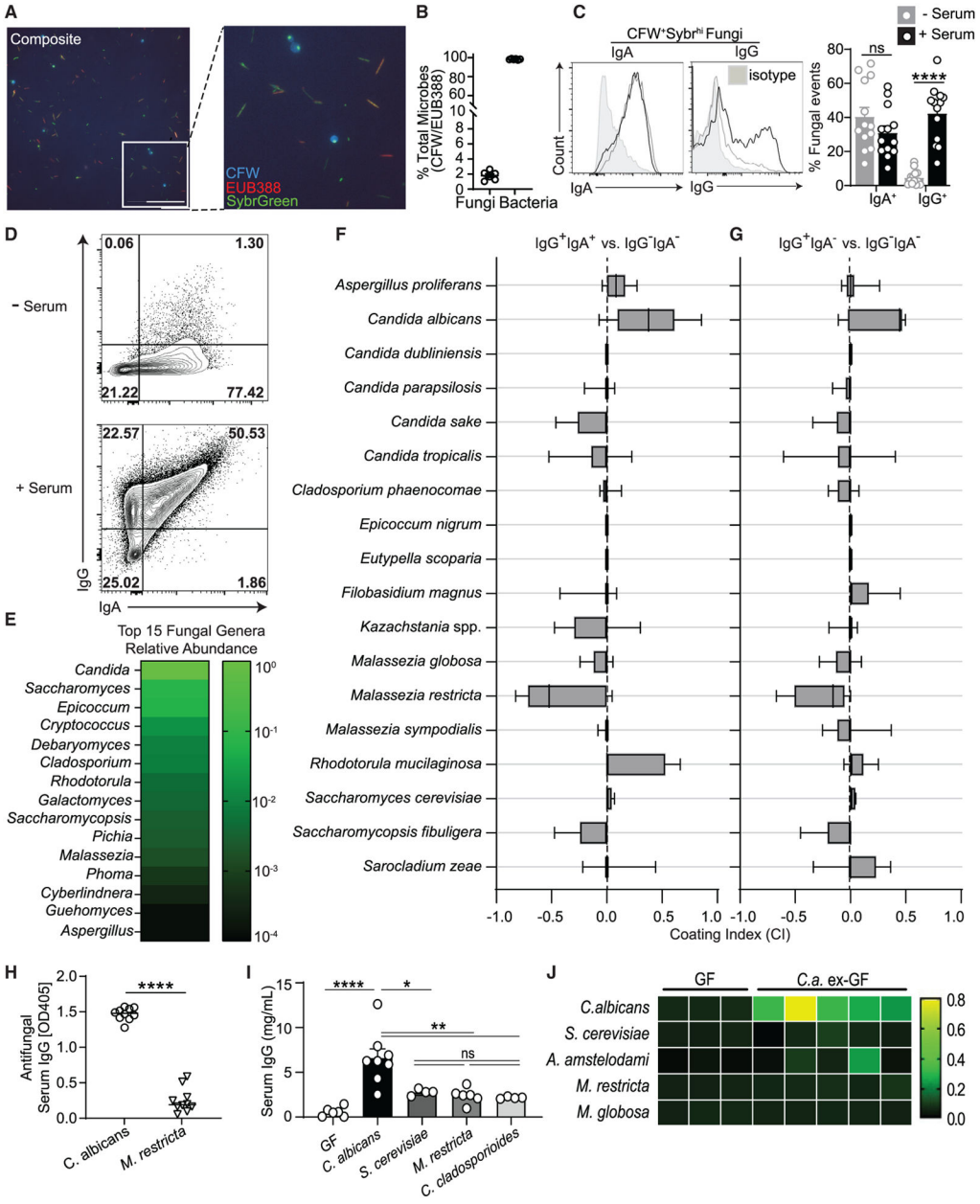

Figure 2. Enrichment of *C. albicans* among IgG-coated intestinal microbes identifies the predominant driver of systemic antifungal IgG responses in humans

(A and B) Visualization of commensal fungi and bacteria in human feces stained with Sybr Green (DNA), CFW (fungal cells), and the EUB338 FISH probe (bacteria); the scale bar represents 25 μm (A). The percentages of fungal ($CFW^+Sybr\ Green^+$) and bacterial ($EUB338^+$ $Sybr\ Green^+$) cells in 6 fecal samples from healthy individuals are shown in (B). Each dot represents an individual feces donor.

(C) Fungi in feces from healthy human donors were assessed for IgA and IgG binding by multiKAP; no serum incubation (gray), incubation with matched serum (black). Mann-Whitney test, n = 13.

(D–G) Combined multiKAP-based sorting and sequencing analysis of antibody-bound species of healthy human mycobiota.

(D) Human feces from healthy donors was incubated with matched serum and assessed for IgA and IgG binding by multiKAP.

(E) Abundance of the top 15 fungal genera in human fecal samples.

(F and G) Relative enrichment of fungal species in antibody-bound fractions, IgG^+IgA^+ (F) or IgG^+IgA^- (G), expressed relative to the IgG^-IgA^- (unbound) population. Confidence interval (CI) values were calculated at the species level. Fungal species represented at 2% or more are depicted. One-sample t test, n = 7. Boxplots represent species' median and the first to third quartiles, and whiskers represent minimum and maximum values. Starred boxplots indicate fungal species with a mean CI significantly greater or less than 0, indicating preferential enrichment in the antibody-bound or unbound fraction. Non-enriched species are unlabeled.

(H) ELISA-based validation of IgG reactivity against fungal lysates from *C. albicans* (recognized by antifungal antibodies; F and G) or *M. restricta* (not recognized by antifungal antibodies; F and G) in healthy human serum. Mann-Whitney test. Human sera, n = 10; each dot represents an individual subject. Each dot represents a serum sample from a healthy individual.

(I) Serum IgG titers in the serum of germ-free (GF) mice monocolonized with the fungal species identified in Figures 2F and 2G, assessed by ELISA. Serum IgG titers of each group are statistically compared relative to uncolonized controls. One-way ANOVA followed by Tukey's multiple comparisons test. Data are representative of three independent experiments. GF, n = 6; *C. albicans*, n = 8; *S. cerevisiae*, n = 4; *M. restricta*, n = 6; *C. cladosporioides*, n = 4. Each dot represents an individual mouse. Error bars indicate SEM. ns, $p \geq 0.05$; *$p < 0.05$; **$p < 0.01$; ***$p < 0.001$; ****$p < 0.0001$.

(J) Serum IgG reactivity from untreated (GF) or *C. albicans*-monocolonized GF mice (*Ca*-exGF) against lysates from *C. albicans*, *S. cerevisiae*, *A. amstelodami*, *M. restricta*, and *M. globosa* pure cultures was measured by ELISA. Squares represent individual mice. Heatmap values represent optical density 405 (OD_{405}) measurements. GF, n = 3; *Ca*-exGF, n = 5. Error bars indicate SEM. ns, $p \geq 0.05$; *$p < 0.05$; **$p < 0.01$; ***$p < 0.001$; ****$p < 0.0001$. See also Figure S2 and Table S1.

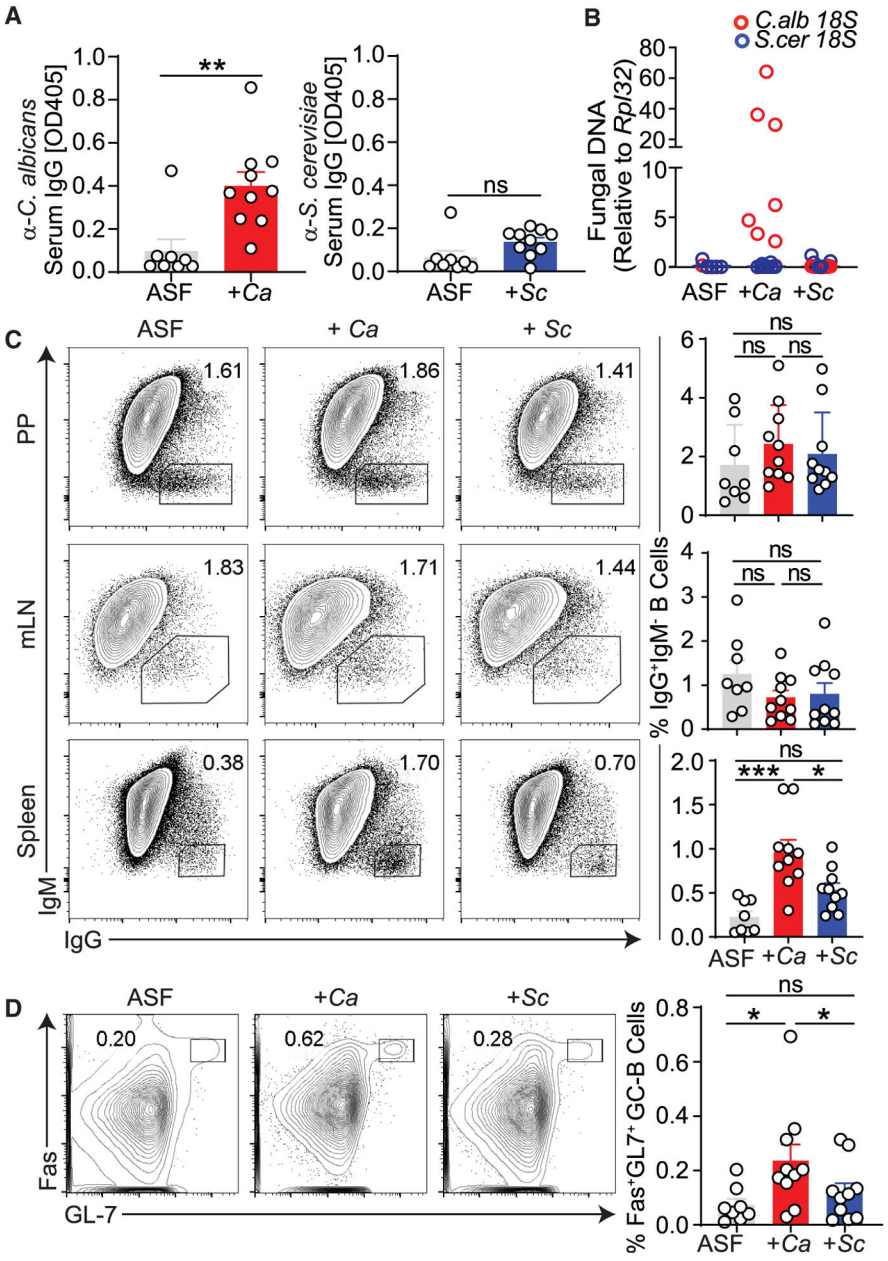

Figure 3. Intestinal *C. albicans* elicits extra-intestinal GC-dependent IgG$^+$ B cell responses

Mycobiota-free altered Schaedler flora (ASF) mice were orally gavaged with PBS (ASF), *C. albicans* (+*Ca*), or *S. cerevisiae* (+*Sc*).

(A) Serum anti-*C. albicans* IgG antibody production in *Ca*-colonized ASF mice (A, left) and serum ASCA production in *Sc*-colonized ASF mice (A, right) compared with ASF controls, as measured by ELISA.

(B) qPCR-based 18S rDNA assessment of spleens from ASF mice colonized for 2 weeks with *C. albicans* or *S. cerevisiae* or left untreated.

(C) Frequency of IgG$^+$IgM$^-$ among CD19$^+$CD4$^-$ B cells in PPs (top), mLNs (center), and spleen (bottom), analyzed by flow cytometry (pooled from two independent experiments).

(D) Frequency of GC-B cells among $CD19^{+}CD4^{-}$ B cells in the spleen, analyzed by flow cytometry. One-way ANOVA followed by Tukey's multiple comparisons test. ASF, n = 8; +*Ca*, n = 10; +*Sc*, n = 10. Data are pooled from three independent experiments.
Each dot represents an individual mouse. Error bars indicate SEM. ns, $p \geq 0.05$; *$p < 0.05$; **$p < 0.01$; ***$p < 0.001$; ****$p < 0.0001$. See also Figure S3 and Table S1.

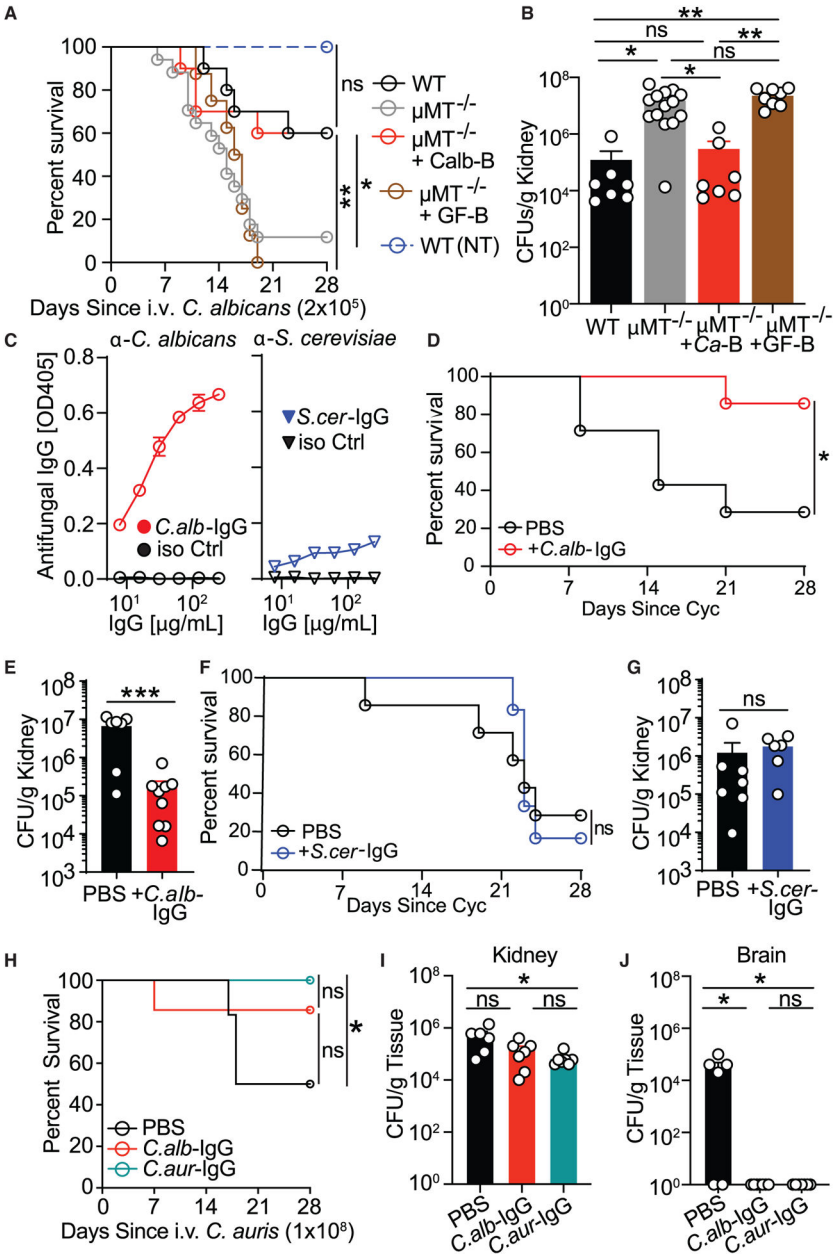

Figure 4. Antibodies induced through intestinal *Candida* colonization confer protection against gut-derived and blood-borne systemic candidiasis caused by *C. albicans* or *C. auris*

(A and B) WT mice (WT), $\mu MT^{-/-}$ mice ($\mu MT^{-/-}$), and $\mu MT^{-/-}$ mice adoptively transferred splenic B cells from *C. albicans*-monocolonized GF mice (m$MT^{-/-}$ +*Ca*-B) or untreated GF mice ($\mu MT^{-/-}$ +GF-B) were infected intravenously (i.v.) with *C. albicans*. A control group of WT mice was left uninfected (WT, NI). Disease morbidity (A) and *C. albicans* systemic spread to kidney tissue (B) were assessed; log rank Mantel-Cox test (A) and one-way ANOVA followed by Tukey's multiple comparisons test (B). WT, n = 7; $\mu MT^{-/-}$, n = 14; $\mu MT^{-/-}$ +*Ca*-B, n = 7; $\mu MT^{-/-}$ +GF-B, n = 8; WT (NI), n = 5. Data are representative of three independent experiments.

(C) Antibody reactivity assessment against *C. albicans* and *S. cerevisiae* lysates of purified serum IgG antibodies from *C. albicans*- (*C.alb*-IgG, left panel) and *S. cerevisiae*- (*S.cer*-IgG, right panel) monocolonized GF mice, respectively measured by ELISA.

(D and E) *C.alb*-IgG protection against cyclophosphamide (Cyc)-induced systemic fungal dissemination in SPF mice intestinally colonized with *C. albicans* (treatment scheme depicted in Figure S4B). Shown are disease morbidity (D) and systemic *C. albicans* spread into kidney tissue (H). Statistical analysis was performed using log rank Mantel-Cox test (D) or Mann-Whitney test (E). PBS, n = 7; *+C.alb*-IgG, n = 9.

(F and G) Lack of protection by *S.cer*-IgG against Cyc-induced systemic fungal dissemination in SPF mice intestinally colonized with *C. albicans* (treatment scheme depicted in Figure S4B). Shown are survival (F) and systemic *C. albicans* spread into kidney tissue (G). ns, $p > 0.05$; log rank Mantel-Cox test (F) and Mann-Whitney test (G). PBS, n = 7; *+C.alb*-IgG, n = 6.

(H–J) Intestinal GF colonization-induced *C.aur*-IgG protects mice against systemic infection with *C. auris*. The effect of *C.alb*-IgG and *C.aur*-IgG was assessed after i.v. infection with *C. auris.* Shown are disease morbidity (H) and systemic *C. auris* spread into kidney (I) and brain tissue (J). Statistical analysis was performed using log rank Mantel-Cox test (H) or one-way ANOVA followed by Tukey's multiple comparisons test (I and J). PBS, n = 6; *+C.alb*-IgG, n = 7; *+C.aur*-IgG, n = 7. Data are representative of two independent experiments.

Each dot represents an individual mouse. Error bars indicate SEM. ns, $p \geq 0.05$; *$p < 0.05$; **$p < 0.01$; ***$p < 0.001$; ****$p < 0.0001$. See also Figure S4.

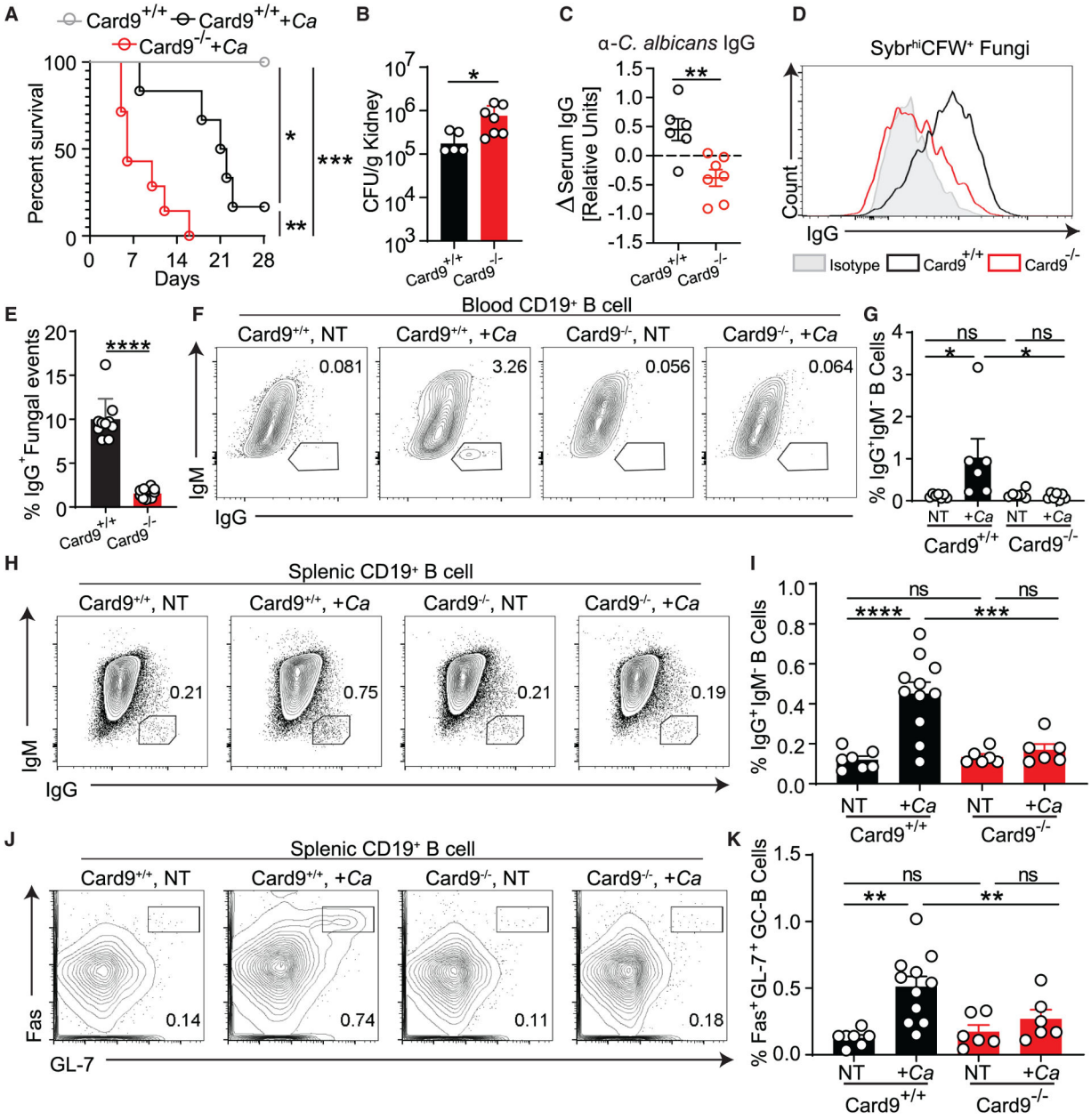

Figure 5. CARD9 is critical for the GC-dependent generation of antifungal IgG antibodies.

(A–C) Cyc-induced gut-to-system fungal dissemination was induced in *Card9*$^{+/+}$ and *Card9*$^{-/-}$ mice.

(A and B) Disease morbidity assessed by survival (A) and *C. albicans* systemic spread to the kidneys (B). *C. albicans* detection failed in one mouse, which was excluded from the analysis.

(C) Change in anti-*C. albicans* serum IgG after mice became moribund (14 days after infection) relative to pre-infection titers.

(D and E) MultiKAP analysis of anti-fungal antibodies in healthy *Card9*$^{+/+}$ and *Card9*$^{-/-}$ mice.

(A–E) Statistical analysis was performed using log rank Mantel-Cox test (A) or Mann-Whitney test (B, C, and E). *Card9*$^{+/+}$, n = 6; *Card9*$^{+/+}$ +Ca, n = 6; *Card9*$^{-/-}$ +Ca, n = 7. Data are representative of two independent experiments.

(F and G) Systemic IgG and B cell responses of *Card9*$^{+/+}$ and *Card9*$^{-/-}$ mice 2 weeks after intraperitoneal injection with *C. albicans*. The B cell compartment in blood samples from individual mice was analyzed by flow cytometry. One-way ANOVA followed by Tukey's multiple comparisons test. *Card9*$^{+/+}$ NT, n = 7; *Card9*$^{+/+}$ +*Ca*, n = 6; *Card9*$^{-/-}$ NT, n = 6; *Card9*$^{-/-}$ +*Ca*, n = 6. Data are representative of two independent experiments.

(H–K) Systemic IgG and B cell responses of *Card9*$^{+/+}$ and *Card9*$^{-/-}$ mice after intraperitoneal injection with *C. albicans*. The B cell compartment in spleen samples from individual mice was analyzed by flow cytometry. One-way ANOVA followed by Tukey's multiple comparisons test. *Card9*$^{+/+}$ NT, n = 7; *Card9*$^{+/+}$ +*Ca*, n = 11; *Card9*$^{-/-}$ NT, n = 6; *Card9*$^{-/-}$ +*Ca*, n = 6. Data are representative of three independent experiments.

Each dot represents an individual mouse. Error bars indicate SEM. ns, $p \geq 0.05$; *$p < 0.05$; **$p < 0.01$; ***$p < 0.001$; ****$p < 0.0001$. See also Figure S4.

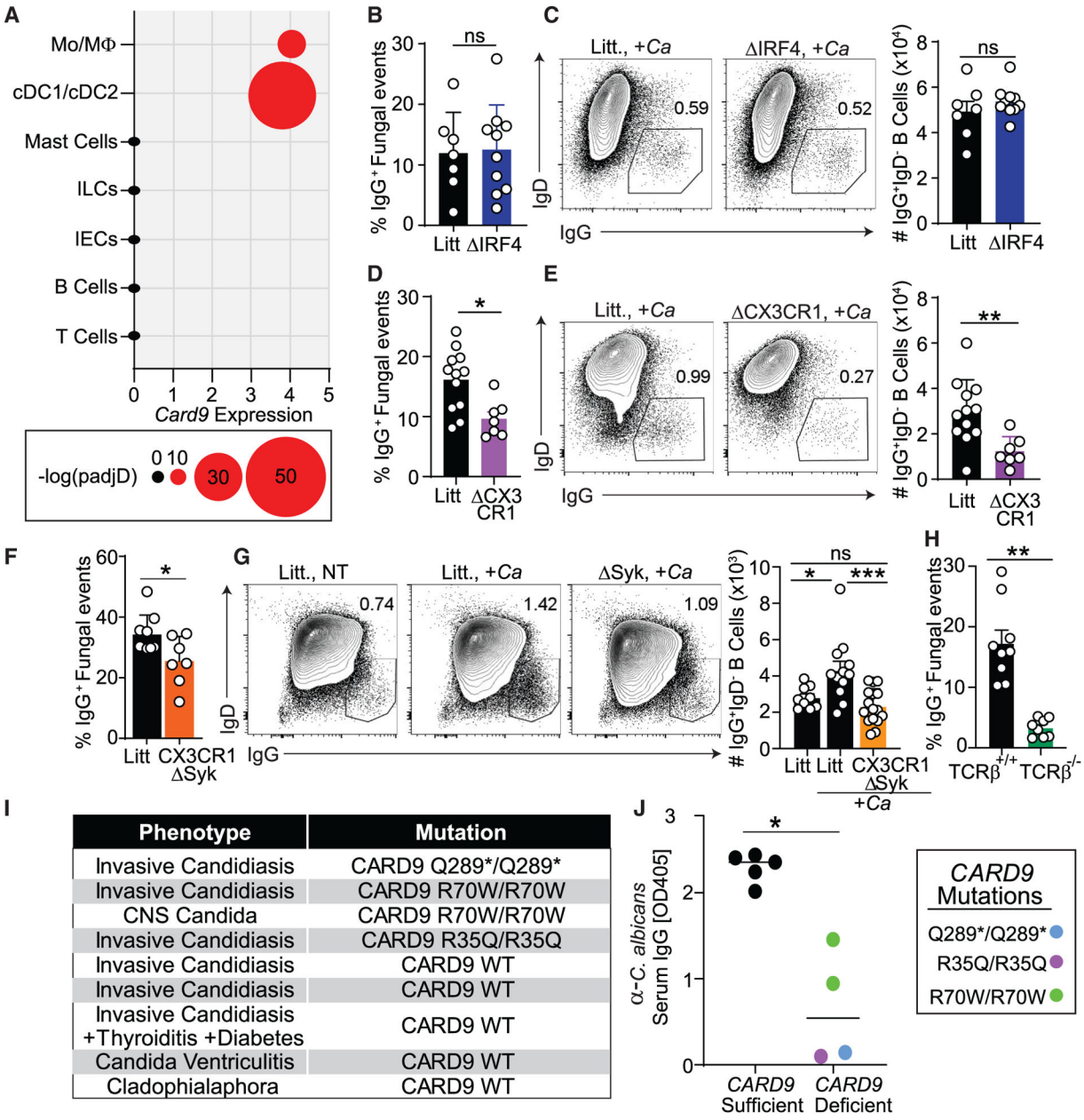

Phenotype	Mutation
Invasive Candidiasis	CARD9 Q289*/Q289*
Invasive Candidiasis	CARD9 R70W/R70W
CNS Candida	CARD9 R70W/R70W
Invasive Candidiasis	CARD9 R35Q/R35Q
Invasive Candidiasis	CARD9 WT
Invasive Candidiasis	CARD9 WT
Invasive Candidiasis +Thyroiditis +Diabetes	CARD9 WT
Candida Ventriculitis	CARD9 WT
Cladophialaphora	CARD9 WT

Figure 6. Syk-CARD9-dependent signaling in CX3CR1$^+$ MNPs is critical for induction of antifungal IgG antibody responses

(A) Single-cell RNA-seq analysis of *CARD9* expression in human biopsies from a single-cell RNA-seq dataset from Smillie et al. (2019).

(B and C) Systemic IgG and B cell responses in ΔIRF4 or littermates (Litt) upon intestinal colonization with *C. albicans*. Data were collected from two independent experiments. Statistical analyses were performed using Mann-Whitney test. Litt, n = 7; ΔIRF4, n = 10.

(B) MultiKAP analysis of anti-fungal antibodies in ΔIRF4 and littermate mice.

(C) Frequency and absolute numbers of IgG$^+$IgD$^-$ among splenic CD19$^+$CD4$^-$ B cells analyzed by flow cytometry.

(D and E) Systemic IgG and B cell responses in ΔCX3CR1 mice and Litt upon intestinal colonization with *C. albicans*. Data were collected from two independent experiments. Statistical analyses were performed using Mann-Whitney test. Litt, n = 12; ΔCX3CR1, n = 7.

(D) MultiKAP analysis of anti-fungal antibodies in ΔCX3CR1 and Litt mice.

(E) Frequency and absolute numbers of $IgG^{+}IgD^{-}$ among splenic $CD19^{+}CD4^{-}$ B cells analyzed by flow cytometry.

(F) Feces of healthy $CX3CR1^{\Delta Syk}$ and Litt were assessed by multiKAP for systemic antifungal IgG binding after incubation with matched sera. Data were collected from two independent experiments; Mann-Whitney test. Litt, n = 8; $CX3CR1^{\Delta Syk}$, n = 7.

(G) Frequency and absolute numbers of $IgG^{+}IgD^{-}$ among splenic $CD19^{+}CD4^{-}$ B cells analyzed by flow cytometry in $CX3CR1^{\Delta Syk}$ and Litt mice after oral gavage with *C. albicans*. Data were collected from three independent experiments; Mann-Whitney test. Litt NT, n = 9; Litt *+Ca*, n = 12; $CX3CR1^{\Delta Syk}$ *+Ca*, n = 16.

(H) MultiKAP analysis of anti-fungal antibodies in healthy $TCR\beta^{+/+}$ and $TCR\beta^{-/-}$ mice. Mann-Whitney test $TCR\beta^{+/+}$, n = 9; $TCR\beta^{-/-}$, n = 8. Data are representative of two independent experiments.

(I and J) Anti-*Candida* IgG antibody titers (J) assessed by ELISA in sera from individuals with candidiasis who were non-carriers or carriers of *CARD9* loss-of-function mutations (Q289*, R35Q, R70W) (I). Non-carriers: *CARD9* sufficient, n = 5; carriers: *CARD9* deficient, n = 4. Each dot represents an individual human subject; Mann-Whitney test. Error bars indicate SEM. ns, $p \geq 0.05$; *$p < 0.05$; **$p < 0.01$; ***$p < 0.001$; ****$p < 0.0001$. See also Figures S5.

KEY RESOURCES TABLE

REAGENT or RESOURCE	SOURCE	IDENTIFIER
Antibodies		
Rat IgG1 kappa Isotype Control (eBRGI), PE	Thermo Fisher Scientific (eBioscience™)	Cat # 12-4301-82; RRID: AB_470047
IgA Monoclonal Antibody (mA-6E1), PE	Thermo Fisher Scientific (eBioscience™)	Cat # 12-4204-82; RRID: AB_465917
Rat IgG2a, k Isotype Control (R35-95), FITC	BD PharMingen™	Cat # 554688
anti-Mouse IgG1 Secondary Antibody (M1-14D12), FITC	Thermo Fisher Scientific (eBioscience™)	Cat # 11-4015-80; RRID: AB_11043272
anti-Mouse IgG2b Secondary Antibody (m2b-25G4), FITC	Thermo Fisher Scientific (eBioscience™)	Cat # 11-4220-80; RRID: AB_2572494
Rat anti-Mouse IgG3 (R40-82), FITC	BD PharMingen™	Cat # 553403
Alexa Fluor® 647 ChromPure Goat IgG, whole molecule	Jackson Immunoresearch	Cat # 005-600-003 RRID: AB_2337016
Alexa Fluor® 647 AffiniPure Goat Anti-Mouse IgG, Fcγ fragment specific	Jackson Immunoresearch	Cat # 115-605-071 RRID: AB_2338909
Rat IgG2a kappa Isotype Control (eBR2a), PE-Cyanine7	Thermo Fisher Scientific (eBioscience™)	Cat # 25-4321-82 RRID: AB_470200
IgM Monoclonal Antibody (Il/41), PE-Cyanine7	Thermo Fisher Scientific (eBioscience™)	Cat # 25-5790-82 RRID: AB_469655
Isotype Control Antibody, mouse IgG1 (IS5-21F5), PE	Miltenyi Biotec	Cat #130-113-200
IgA Antibody, anti-human (IS11-8E10), PE	Miltenyi Biotec	Cat # 130-113-476
Goat IgG-Alexa Fluor® 647	Southern Biotech	Cat #0109-31
Goat Anti-Human IgG-Alexa Fluor® 647	Southern Biotech	Cat # 2040-31
CD16/CD32 monoclonal antibody (93), eBioscience	Thermo Fisher Scientific (eBioscience™)	Cat #14-0161-81; RRID: AB_467132
eBioscience™ Fixable Viability Dye eFluor™ 455UV	Thermo Fisher Scientific (Invitrogen™)	Cat #65-0868-18
Brilliant Violet 650™ anti-mouse CD45 Antibody (30-F11)	Biolegend	Cat # 103151; RRID: AB_2565884
Brilliant Violet 605™ anti-mouse CD4 Antibody (RM4-5)	Biolegend	Cat # 100548; RRID: AB_2563054
Alexa Fluor® 700 anti-mouse CD19 Antibody (6D5)	Biolegend	Cat # 115527; RRID: AB_493734
BV510 Rat Anti-Mouse IgD (11-26c.2a)	BD Horizon™	Cat #563110
IgM Monoclonal Antibody (Il/41), FITC	Thermo Fisher Scientific (eBioscience™)	Cat # 11-5790-81; RRID: AB_465244
PE-Cy™7 Hamster Anti-Mouse CD95 (Jo2)	BD PharMingen™	Cat # 557653
Pacific Blue™ anti-mouse/human GL7 Antigen (T and B cell Activation Marker) Antibody	Biolegend	Cat # 144613; RRID: AB_2563291
eBioscience Fixable Viability Dye eFluor 506	Thermo Fisher Scientific (eBioscience™)	Cat #65-0866-14
Brilliant Violet 605™ Anti-mouse I-A/I-E a (M5/114.15.2)	BioLegend	Cat # 107639; RRID: AB_2565894
Anti-mouse CD11b monoclonal antibody (M1/70), PE-Cyanine7	Thermo Fisher Scientific (eBioscience™)	Cat # 25-0112-82; RRID: AB_469588
Anti-mouse CX3CR1 antibody (SA011F11), BV421	BioLegend	Cat #149023; RRID: AB_2565706
Anti-mouse CD11c antibody (N418), Alexa Fluor 700	BioLegend	Cat # 117319; RRID: AB_528735
CD103 (Integrin alpha E) Monoclonal Antibody (2E7) PerCP-eFluor 710	Thermo Fisher Scientific (eBioscience™)	Cat # 46-1031-82; RRID: AB_2573704
Anti-Mouse IgG IgA IgM (H+L antibody) produced in goat	Sigma-Aldrich (Millipore)	Cat # SAB3701043-2MG

REAGENT or RESOURCE	SOURCE	IDENTIFIER
Goat Anti-Human Ig-UNLB	Southern Biotech	Cat # 2010-01; RRID: AB_2687525
Mouse Reference Serum	Bethyl Laboratories	Cat # RS10-101
Human IgG-UNLB	Southern Biotech	Cat # 0150-01; RRID: AB_2794075
Alkaline Phosphotase AffiniPure F(ab')$_2$ Fragment Goat Anti-Mouse IgG, Fcγ fracgment specific	Jackson Immunoresearch	Cat # 115-056-071; RRID: AB_2338553
Alkaline Phosphatase AffiniPure F(ab')$_2$ Fragment Goat Anti-Human IgG, Fcγ fragment specific	Jackson Immunoresearch	Cat # 109-056-098; RRID: AB_2337618
Bacterial and fungal strains		
Altered Schaedler Flora (ASF)	N/A	PMID: 14325473
Candida albicans SC5314	ATCC	ATCC MYA-2876)
Saccharomyces cerevisiae Meyen ex E.C. Hansen	ATCC	ATCC MYA-796
Cladosporium cladosporioides	ATCC	ATCC 38810
Malassezia restricta	ATCC	ATCC MYA-4611
Candida auris	CDC	CDC0389
Chemicals, peptides, and recombinant proteins		
Sybr Green Nucleic Acid Gell Stain - 10,000X concentrate in DMSO	Thermo Fisher Scientific (Invitrogen™)	Cat # S7563
Calcofluor White Stain	Sigma-Aldrich (Millipore)	Cat # 18909
DAPI (4', 6-Diamidino-2-Phenyldole, Dihydrochloride)	Thermo Fisher Scientific (Invitrogen™)	Cat # D1306
Propidium Iodide - 1.0 mg/mL Solution in Water	Thermo Fisher Scientific (Invitrogen™)	Cat # P3566
Bovine Albumin Fraction V	MP Biomedicals	Cat# IC820451
Hanks' balanced salt solution (HBSS)	Sigma	Cat # H4385
Fetal Bovine Serum	Corning	Cat# MT35016CV
RPMI 1640 with L-glutamine	Corning	Cat # 45000-396
Sabouraud dextrose broth	VWR	Cat# 89406-400
Sabouraud 4% dextrose agar	VWR	Cat # EM1.05438.0500
Penicillin-Streptomycin (10,000 U/mL)	Thermo Fisher Scientific	Cat # 15140122
Tween® 80 (Polysorbate)	VWR	Cat # 97061-674
Cefoperazone sodium salt	Sigma	Cat # C4292-5G
Cyclophosphamide	Thermofisher Scientific (Tocris Bioscience™)	Cat #40-915-0
RBC Lysis Buffer (10X)	Biolegend	Cat # 420301
Citrate-dextrose solution (ACD)	Sigma-Aldrich (Millipore)	Cat # C3821-50ML
Fluconazole	Sigma-Aldrich (Millipore)	Cat # PHR1160-1G
Penicillin G sodium salt	Sigma-Aldrich (Millipore)	Cat # PENNA-10MU
Streptomycin Sulfate, 25 Grams	Research Products International	Cat #3810-74-0
Gentamycin Sulfate, 1 Gram	Research Products International	Cat # 1405-41-0
Standard flagellin from S. *typhimurium*	Invivogen	Cat # tlrl-stfla
Mannan from *Saccharomyces cerevisiae*	Sigma-Aldrich (Millipore)	Cat # M7504-100MG
pNPP Powder	Thermo Fisher Scientific (Invitrogen™)	Cat # 002201

REAGENT or RESOURCE	SOURCE	IDENTIFIER
Critical commercial assays		
B Cell Isolation Kit, Mouse	Miltenyi	Cat # 130-090-862
Protein G UltraLink™ Columns, 2mL	Thermofisher Scientific (Pierce™)	Cat #53127
Amicon Ultra-15 Centrifugal Filter Unit	Sigma-Aldrich (Millipore)	Cat # UFC900308
Deposited data		
ITS Sequencing	NCBI	https://www.ncbi.nlm.nih.gov/sra/docs/ Bioproject ID: PRJNA630985
Experimental models: organisms/strains		
Mouse: C57BL/6	The Jackson Laboratory	JAX# 000664
Mouse: B6.129S2-Ighm^{tm1Cgn}/J	The Jackson Laboratory	JAX# 002288
Mouse: B6.Cg-Tg(Itgax-cre)1-1Reiz/J	The Jackson Laboratory	JAX# 008068
Mouse: B6.129S1-Irf4^{tm1Rdf}/J	The Jackson Laboratory	JAX# 009380
Mouse: B6N.129P2-Cx3cr1$^{tm3(DTR)Litt}$/J	The Jackson Laboratory	JAX# 025629
Mouse: B6.129P2-Syk$^{tm1.2Tara}$/J	The Jackson Laboratory	JAX# 017309
Mouse: B6.129P2(Cg)-Cx3cr1 $^{tm2.1(cre/ERT2)Litt}$/WganJ	The Jackson Laboratory	JAX# 021160
Mouse: B6.129-Card9^{tm1Xlin}/J	Xin Lin Laboratory	N/A
Mouse: B6(Cg)-*Rag2*$^{tm1.1Cgn}$/J	The Jackson Laboratory	JAX# 008449
Mouse: B6.129P2-*Tcrb*^{tm1Mom}/J	The Jackson Laboratory	JAX# 002118
Oligonucleotides and FISH probe		
18S forward primer for qPCR: 5′-GGRAAACTCACCAGGTCCAG −3′	Liu et al., 2012	N/A
18S reverse primer for qPCR: 5′- GSWCTATCCCCAKCACGA −3′	Liu et al., 2012	N/A
Probe 5′-TGGTGCATGGCCGTT-3′	Liu et al., 2012	N/A
16S rRNA Eubacteria Probe EUB338: 5′- /5Cy5/GCT GCC TCC CGT AGG AGT −3′	Daims et al., 1999	N/A
Software and algorithms		
GraphPad Prim 8.3.0 (538)	GraphPad Software	N/A
RStudio Desktop 1.1.463	https://rstudio.com/	N/A
R version 3.4.4 (2018-03-15)	https://www.r-project.org	N/A
FlowJo LLC 10.1.	Becton Dickinson	N/A